Nucleon Resonance Structure Studies Via Exclusive KY Electroproduction at 6.6 GeV and 8.8 GeV

Experimental Support

Daniel S. Carman *(Contact Person, Spokesperson)*, Victor Mokeev *(Spokesperson)*,
Harut Avakian, Volker Burkert, Kijun Park, Eugene Pasyuk
Jefferson Laboratory, Newport News, VA 23606, USA

Gleb Fedotov, Ralf Gothe *(Spokesperson)*, Iuliia Skorodumina
University of South Carolina, Columbia, SC 29208, USA

Bill Briscoe
The George Washington University, Washington, DC 20052, USA

Dave Ireland
University of Glasgow, Glasgow G12 8QQ, United Kingdom

Brian Raue
Florida International University, Miami, FL 33199

Evgeny Golovach, Boris Ishkhanov, Evgeny Isupov
Skobeltsyn Nuclear Physics Institute, Moscow State University, 119899, Moscow, Russia

Haiyun Lu
University of Iowa, Iowa City, IA 52242

Ken Hicks
Ohio University, Athens, OH 45701

Annalisa D'Angelo, Lucilla Lanza
Universitá di Roma Tor Vergata and INFN Roma Tor Vergata, 00133 Rome, Italy

and the CLAS Collaboration

A New Experiment Run Group Proposal Submitted to Jefferson Lab PAC44

Theoretical Support

Robert G. Edwards, Michael R. Pennington, David G. Richards, Adam P. Szczepaniak[†]
Theory Center, Jefferson Laboratory, Newport News, VA 23606, USA
([†]*Joint with Indiana University, Bloomington, IN 47405*)

Hiroyuki Kamano
KEK Theory Center, Institute of Particle and Nuclear Studies, High Energy Accelerator Research Organization, Tsukuba, Ibaraki 305-0801, Japan

Michael Döring, Igor Strakovsky, Ron Workman
The George Washington University, Washington, DC 20052, USA

T.-S. Harry Lee, Craig D. Roberts
Argonne National Laboratory, Argonne, IL 60439, USA

Jan Ryckebusch
Ghent University, B-9000 Ghent, Belgium

Elena Santopinto
INFN Sezione di Genova, 16146 Genova, Italy

César Fernández-Ramírez
Instituto de Ciencias Nucleares, Universidad Nacional Autónoma de México, A.P. 70-543, México D.F. 04510, México

June 2, 2016

A New Experiment Run Group Proposal Submitted to Jefferson Lab PAC44

CLAS12 Run Group K

Quark-Gluon Confinement & Strong QCD Executive Summary

Run Group Coordinator: V. Burkert

The proposals listed below are part of the CLAS12 **Run Group K**. They have been separately submitted for PAC44 approval. As a Run Group they are using the same run conditions and the same CLAS12 configuration and will take data together as a group.

- A Search for Hybrid Baryons in Hall B with CLAS12 - Contact Person: A. D'Angelo
- Deeply Virtual Compton Scattering with CLAS12 at 6.6 GeV and 8.8 GeV - Contact Person: L. Elouadrhiri
- Nucleon Resonance Structure Studies Via Exclusive KY Electroproduction at 6.6 GeV and 8.8 GeV - Contact Person: D.S. Carman
- Additional experimental aspects that address strong QCD and confinement aspects discussed in Sections A, B, and C below.

The search for hybrid baryons is the primary program that is setting the experimental conditions such as the electron beam energies E_b=6.6 GeV and 8.8 GeV with fully longitudinally polarized electrons ($P_b \geq 85\%$) impinging on a liquid-hydrogen target with a beam current equivalent to a luminosity of $L = 10^{35}$ cm^{-2}s^{-1}. The polarity and strength of the Torus magnetic field in CLAS12 is set by the current in the superconducting Torus coils at I=-3375 A, i.e. electrons bending away from the beamline.

Brief Summary

This series of Run Group proposals aims at establishing a comprehensive research program to tackle some of the most intricate problems in hadron physics. They have also strong connections to proposals that have already been approved as part of the CLAS12 physics program and will very significantly extend the science reach of those experiment, while at the same time presenting new avenues towards clarifying the degrees of freedom active in the excitation of baryons and providing new insight into the so far unresolved problem of understanding the confinement of light quarks. The scope of this program covers three major research efforts:

- Establishing the nucleon excitation spectrum with emphasis on the high mass region and gluonic excitations;
- Quantifying the role of the active degrees of freedom in the nucleon spectrum and their evolution with distance scale;
- Making inroads towards understanding the confinement of light quarks, gluons, and the meson cloud, their emergence from the confinement regime, and the role they have in providing dynamical stability of the nucleon.

The tools available to meet these challenges that will be employed in this Run Group proposal are:

- Extending and completing our knowledge of the nucleon energy spectrum by measurement of a variety of processes and final states. This also includes use of modern analysis tools in multi-channel partial wave analysis, as well as reaction models for specific channels such as $N\pi$, $N\pi\pi$, KY that have been developed in the recent past.

- Determining the transition form factors and their Q^2 dependence in exclusive meson electroproduction, and their interpretation in terms of quark excitations, gluonic excitations, or dynamically generated excitations. This involves the strong theory effort provided by the group of participating theorists. Several lower mass states have already been successfully interpreted in such categories.

- Providing new insight into the confinement of light quarks by measuring the shear forces and pressure distributions on quarks by employing the DVCS process to extract the chiral even GPDs $H(x,\xi,t)$ and $E(x,\xi,t)$. This opportunity is provided by the very remarkable properties of the second moments of GPDs H and E that relate to the gravitational form factors $d_1(t)$ and $M_2(t)$ of the nucleon matrix element of the energy-momentum tensor. These form factors can only be measured directly in graviton-nucleon scattering.

Significant progress has been made in recent years and is evident in several new entries of N^* and Δ^* states in the latest editions of the Review of Particle Properties (PDG), as well as the inclusion of the transition form factor measurement for several excited states. Most of the newly discovered states have masses in the range 1.85 GeV to 2.1 GeV where precise photoproduction data were driving the new observations, and we may expect additional new states to be observed from the data sets that are still in the analysis phase, and therefore have not been included in the available multi-channel analysis frameworks. However, the mass region above 2.1 GeV has hardly been studied. This is the region where the gluonic excitations are expected to occur, and it is a major focus of this Run Group. Additionally, measuring concurrently a set of different final states opens up new possibilities that were not available with the configuration available with the CLAS detector in the lower energy range. Some of these are discussed in the following sections.

A. Excited Nucleon Structure Studies at Low Q^2

Besides the search for hybrid baryon states, there are many open issues in our knowledge of the structure of ordinary baryon excitations that can be addressed in parallel with the data taken during the beam time from this proposed new Run Group at E_b=6.6 GeV and 8.8 GeV.

The electrocouplings of the $N(1680)\frac{5}{2}^+$ resonance [1], the strongest state in the third nucleon resonance region, is one example. The data from different exclusive channels are quite sparse and the high-statistics data expected from this experiment for $Q^2 \leq 2.0$ GeV^2 would remedy the lack of experimental information in that kinematic range and address similar situations for other states as well. Note that the approved JLab experiment E12-09-003 [2] will focus on the high-Q^2 extension of the resonance studies.

Another compelling example is the $N(1675)\frac{5}{2}^-$ state, where data at $Q^2 > 1.8$ GeV^2 have been published recently by the CLAS Collaboration [1]. Low Q^2 data are very important here, as for this state the quark transitions from a proton are strongly suppressed by the Moorhouse selection rule, and therefore, any non-zero value of the electrocoupling amplitudes will directly measure the strength of the meson-baryon contributions.

In general, the studies of resonance electrocouplings at small photon virtualities down to 0.5 GeV^2 will allow us to access meson-baryon contributions with unprecedented precision and scope, and at $Q^2 \leq 0.5$ GeV^2, as proposed in this experiment, they will allow us for the first time to explore their Q^2 evolution at distance scales where the meson-baryon cloud contributions are maximal, offering preferential conditions for the exploration of this component of N^* structure. Furthermore, the proposed experiment opens up the possibility to explore the longitudinal $\gamma_v pN^*$ electrocouplings at photon virtualities down to Q^2=0.05 GeV^2.

Recent advances in the studies of nucleon structure using the QCD-based Dyson-Schwinger equations have provided strong indications that quark-gluon confinement in the real-world is a dynamical process and point to an intimate connection between confinement and Dynamical Chiral Symmetry Breaking (DCSB) [3,4]. Moreover, in providing a clear explanation of the dichotomous nature of pions, as both bound-states of massive constituents and Nambu-Goldstone bosons, these studies force a realization that baryons constituted from fully-dressed confined-quarks must also be surrounded by a complex meson-baryon cloud, generated by a sequence of meson-baryon final-state interactions. A detailed understanding of the interplay between the dressed-quark core in a diverse array of nucleon excited states and the associated meson-baryon clouds is crucial to developing a quantitative picture of the dynamical confinement mechanism. This understanding requires a systematic investigation of resonance electrocouplings at low virtuality. The studies proposed herein will therefore address a critical open problem in hadron physics, namely, exposing those features of the hadronization process that control the transition from the quark-gluon color-confinement regime to the asymptotic domain of strong interactions between color-neutral mesons and baryons.

The extension of exclusive photoproduction to electroproduction data at small Q^2 with maximal statistical accuracy is of particular importance in the search of new baryon states. A successful combined description of exclusive photo- and electroproduction data with the same Q^2-independent resonance mass, width, and partial hadronic decay widths to different final hadron states, will offer strong and almost model-independent evidence for the existence of any new states.

The recent combined analysis [5] of the CLAS $\pi^+\pi^- p$ photoproduction [6] and electroproduction [7] data exemplifies this strength as it revealed further evidence for a new $N'(1720)\frac{3}{2}^+$ baryon state. This state has the same spin-parity and almost the same mass and total decay width as the conventional $N(1720)\frac{3}{2}^+$, but a distinctively different Q^2 dependence of the resonance electrocouplings and partial hadronic decay widths to the $\pi\Delta$ and ρp final states. As shown in the hybrid baryon search proposal, the electrocouplings of the $N(1720)\frac{3}{2}^+$ and $N'(1720)\frac{3}{2}^+$ states evolve for $Q^2 < 1.5$ GeV^2 in a completely different manner. Therefore, the future results on the $N(1720)\frac{3}{2}^+$ and $N'(1720)\frac{3}{2}^+$ state electrocouplings from the data on exclusive $\pi^+\pi^- p$ electroproduction off the proton at small Q^2 will shed light on the differences in the structure of the conventional and the "missing" baryon states.

The studies of exclusive KY and $\pi^+\pi^-p$ electroproduction at W up to 2.5 GeV carried out in the multiple Q^2 bins will enable us to verify the signals of around ten new baryon states by the global multi-channel analysis of exclusive photoproduction data recently carried out by the Bonn-Gatchina group that have been classified by the Particle Data Group [8] as two or three-star resonances.

B. Exclusive K^*Y and KY^* Final States

A cornerstone experiment of this new Run Group is the nucleon structure studies from analysis of the exclusive strangeness channels $K^+\Lambda$ and $K^+\Sigma^0$ in the range of photon virtualities Q^2 from 2.0 GeV^2 to 7.0 GeV^2. These reaction channels were chosen because they have the largest cross sections and the highest acceptances of the various strangeness channels. However, the data taken for this experiment will also nicely allow for studies of strangeness channels with smaller cross sections and detector acceptances. Among the considered reactions include:

$$\begin{aligned} e + p &\rightarrow e' + K^{*+} + \Lambda \\ e + p &\rightarrow e' + K^{*+} + \Sigma^0 \\ e + p &\rightarrow e' + K^{+} + \Lambda(1405) \\ e + p &\rightarrow e' + K^{+} + \Lambda(1520) \\ e + p &\rightarrow e' + K^{+} + \Sigma^0(1385) \\ e + p &\rightarrow e' + K^0_s + \Sigma^+ \\ e + p &\rightarrow e' + K^{*0} + \Sigma^+. \end{aligned}$$

The yield estimates for each of these reaction channels relative to the $K^+\Lambda$ channel for the $e'K^+$ topology in the region of W from 1.8 GeV to 3.0 GeV are expected to be at the 0.5% $\rightarrow$ 2.0% level. For the expected statistics, the yields will be more than an order of magnitude larger than the yields from the existing CLAS data sets. It is expected that they will be sufficient to measure differential cross sections in bins of Q^2, W, and $\cos\theta^*_K$.

The basic motivations to study these different reaction processes include:

- Present coupled channel analyses have been focused mainly on fits to data of πN, ηN, and KY production. However, studies of the K^*Y channels are also expected to provide unique and relevant information regarding production of high-lying N^* states as these final states have not been studied in electroproduction in any detail. The quark model calculations of Ref. [9] showed that several N^* states are predicted to couple to the KY and K^*Y channels with similar strength. These include the $N(2080)\frac{3}{2}^-$, $N(2090)\frac{1}{2}^-$, and $N(2190)\frac{7}{2}^-$. Comparisons of the K^+Y and $K^{*+}Y$ cross sections for these states will be relevant to study the different production mechanisms involved.

- The $\Lambda(1405)$ is situated just below the $N\bar{K}$ threshold and has been an enigmatic state in the spectrum of strange baryons for many years. Only recently have precision photoproduction data from CLAS become available that have started to shed some light on the production dynamics [10,11]. The $\Lambda(1405)$ sits between the $\Sigma(1385)$ and the $\Lambda(1520)$ hyperons. Simultaneous studies of all three states should be expected to

yield insight into their production dynamics, which should lead to further insight into their structures. To date the available theoretical models that have studied $N^* \to KY^*$ decays have produced mixed results on whether s-channel resonance contributions play any significant role [12-15].

- Study of the strangeness production of different isospin partners in the final state, namely Σ^+ production vs. Σ^0 production, is also a necessary part of developing complete reaction models. For example, the dynamics of K^{*0} production are simplified relative to K^{*+} production as K^{*0} exchange in the t-channel is strongly suppressed [16]. Thus studies of both the charged and neutral mesons in the final state may allow for scrutiny of the developed reaction models that can give additional insight into the different isospin channels and their coupling to the final state N^*s.

C. Vector/Pseudoscalar Meson Production at Low Q^2

The running and trigger conditions assumed for the three experiment proposals that compose the present Run Group, allow for the extraction of the unseparated and beam polarization interference terms for vector mesons (ϕ and ω) and pseudoscalar mesons (η') electroproduction on the proton.

The η' meson is an isospin singlet and its production on the proton may occur through the excitation of intermediate N^* resonances only, acting as isospin filter. To date, CLAS has provided two high statistics photoproduction measurements of the $\eta' p$ final state [17,18]. The differential cross section reported for a range of photon energies from 1.5 GeV to 2.2 GeV possess much greater accuracy than previous measurements. Analyses of these data suggest for the first time the coupling of the $\eta' N$ channel to both the $N(1535)\frac{1}{2}^-$ and $N(1710)\frac{1}{2}^+$ resonances, which are known to couple strongly to the ηN channel in photoproduction on the proton. Further, there were hints of important couplings to $J = \frac{3}{2}$ resonances in the process. The high statistics quasi-real electroproduction data collected during this new Run Group offers the possibility to improve the reliability of the results on $\gamma_v p N^*$ electrocouplings in the independent analysis of $\eta' N$ electroproduction.

Vector meson electroproduction is dominated by diffractive production in the t-channel but it is sensitive to baryon excitations at larger momentum transfer. ϕ photoproduction from analysis of data taken at LEPS [19] showed evidence of a localized bump in the differential cross section when a simple Pomeron exchange model predicted a smooth rise from threshold. This feature was also seen in the higher statistics photoproduction data from CLAS in the forward angle differential cross sections at W=2.2 GeV [20]. This bump has been discussed as a possible equivalent to the hidden charm "pentaquark" observed at the LHCb. Other explanations for the bump have been put forward. The first is due to a coupling between the ϕp and $K^+\Lambda(1520)$ channels [21.22]. In this kinematic regime the $\phi p \to K^+K^-p$ charged mode and the $K^+\Lambda(1520) \to K^+pK^-$ decay model have the same final states, and thus rescattering effects can occur between the two channels. The second explanation is due to a $J^P = \frac{3}{2}^-$ N^* resonance with a mass of 2.10±0.03 GeV and width of 0.465±0.141 GeV [23,24]. This purported N^* resonance is such that the ratio of its $A_{1/2}$ to $A_{3/2}$ electrocouplings differs is notably different that the ratio for the $N(2080)\frac{3}{2}^-$ resonance. The effect can be investigated further from the data collected from this Run Group allowing

for a detailed mapping of the Q^2 evolution of the cross section to determine whether the resonance explanation is tenable.

High statistics measurements of the ω meson photoproduction off the proton have been completed with the CLAS detector. These data have provided differential cross section in the range of W from threshold to 2.8 GeV [25]. Based on these data a partial wave analysis was completed [26] that showed the dominant resonance contributions were the $N(1680)\frac{5}{2}^+$ and $N(1700)\frac{3}{2}^-$ states near threshold, as well as the $N(2190)\frac{7}{2}^-$ at higher energies. Further suggestive evidence of a missing $J^P = \frac{5}{2}^+$ state near 2 GeV was also found. Further studies of the resonance contributions that couple to the ω meson as a function of Q^2 from this data set provide a unique opportunity to further our understanding of the dynamics of this process and to probe the structure of the contributing N^* states.

Experimental results in the third resonance region at low Q^2 of these reactions are sparse or non-existent, but are expected to provide new crucial information on the hadrons structure, far from the deeply virtual region, where the virtual photoabsorption occurs on single partons only.

References

[1] K. Park *et al. (CLAS Collaboration)*, Phys. Rev. C **91**, 045203 (2015).

[2] JLab Experiment E12-09-003, spokespersons: V.D. Burkert, P. Cole, R. Gothe, K. Joo, V. Mokeev, P. Stoler

[3] C.D. Roberts, J. Phys. Conf. Ser. **630**, 012051 (2015).

[4] C.D. Roberts and J. Segovia, arXiv:1603.02722 [nucl-th].

[5] V.I. Mokeev *et al.*, Eur. Phys. J. Web Conf. **113**, 01013 (2016).

[6] E. Golovach *et al.*, $\gamma p \to p\pi^+\pi^-$ cross sections from g11a experiment, CLAS Analysis Note (in preparation), (2016).

[7] M. Ripani *et al. (CLAS Collaboration)*, Phys. Rev. Lett. **91**, 022002 (2003)

[8] See http://pdg.lbl.gov/2015/reviews/rpp2015-rev-n-delta-resonances.pdf

[9] S. Capstick and W. Roberts, Phys. Rev. D **58**, 074011 (1998).

[10] K. Moriya *et al. (CLAS Collaboration)*, Phys. Rev. C **87**, 035206 (2013).

[11] K. Moriya *et al. (CLAS Collaboration)*, Phys. Rev. C **88**, 045201 (2013).

[12] Y.Oh, C.M. Ko, and K. Nakayama, Phys. Rev. C **77**, 045204 (2008).

[13] S.-I. Nam, A. Hosaka, and H.-C. Kim, Phys. Rev. D **71**, 114012 (2005).

[14] J. He and X.-R. Chen, Phys. Rev. C **86**, 035204 (2012).

[15] S.-I. Nam, J.-H. Park, A. Hosaka, and H.-C. Kim, J. Korean Phys. Soc. **59**, 2676 (2011).

[16] Q. Zhao, J.S. Al Khalili, and C. Bennhold, Phys. Rev. C **64**, 052201 (R) (2001).

[17] M. Dugger *et al. (CLAS Collaboration)*, Phys. Rev. Lett. **96**, 062001 (2006).

[18] M. Williams *et al. (CLAS Collaboration)*, Phys. Rev. C **80**, 045213 (2009).

[19] T. Mibe *et al. (LEPS Collaboration)*, Phys. Rev. Lett. **95**, 182001 (2005).

[20] B. Dey *et al. (CLAS Collaboration)*, Phys. Rev. D **89**, 055208 (2014).

[21] S. Ozaki, A. Hosaka, H. Nagahiro, and O. Scholten, Phys. Rev. C **80**, 035201 (2009).

[22] H.-Y. Ryu *et al.*, Prog. Theor. Exp. Phys., 023D03 (2014).

[23] A. Kiswandhi, J.J. Xie, and S.N. Yang, Phys. Lett. B **691**, 214 (2010).

[24] A. Kiswandhi and S.N. Yang, Phys. Rev. C **86**, 015203 (2012).

[25] M. Williams *et al. (CLAS Collaboration)*, Phys. Rev. C **80**, 065209 (2009).

[26] M. Williams *et al. (CLAS Collaboration)*, Phys. Rev. C **80**, 065208 (2009).

Proposal Abstract

We propose to use the CLAS12 spectrometer to study $K^+\Lambda$ and $K^+\Sigma^0$ electroproduction from an unpolarized proton target with a longitudinally polarized electron beam at beam energies of 6.6 GeV and 8.8 GeV. The data will be analyzed to measure the differential cross sections, the separated structure functions σ_U, σ_{LT}, σ_{TT}, and $\sigma_{LT'}$, and the hyperon induced and beam-recoil transferred polarizations. The experiment requests 100 days of beam time, 50 days at 6.6 GeV and 50 days at 8.8 GeV.

The goal is to study the spectrum and structure of high-lying nucleon excited states (N^*). Exclusive final states will be measured, including the identification of the scattered electron, the electroproduced K^+, and the p from the hyperon decay. From these data a reaction model will be used to extract the $\gamma_v NN^*$ electromagnetic transition form factors for the most prominent N^* and Δ^* states decaying to KY in the range of invariant energy W from 1.6 GeV to 3 GeV and momentum transfer Q^2 from 2 GeV^2 to 7 GeV^2.

This experiment is an essential component of a comprehensive program of exclusive electroproduction measurements with CLAS12 studying decays of N^* states to a number of different final state channels including πN, ηN, $\pi\pi N$, and KY, and serves as a lower-energy extension of E12-06-108A that was designed to study KY electroproduction at a beam energy of 11 GeV to probe N^* excitation at Q^2 up to 12 GeV^2. The CLAS12 N^* program is designed to explore the evolution of the active degrees of freedom in N^* states, from the regime of meson-baryon dressing and quark-core contributions at lower Q^2 to the regime where dressed quark contributions predominate at higher Q^2, in order to gain unique access to the non-perturbative strong interactions between dressed quarks in excited nucleons of different quantum numbers and to explore the emergence of the meson-baryon cloud from the quark-gluon confinement regime.

Contents

1 Introduction

Intensive spectroscopy of the nucleon excitation spectrum and detailed studies of the structure of these excited states have played a pivotal role in the development of our understanding of the strong interaction. The concept of quarks that emerged through such studies led to the development of the constituent quark model [1, 2] (CQM) in the 1980s. As a result of intense experimental and theoretical efforts over the past 30 years, it is now apparent that the structure of the states in the nucleon excitation spectrum provides important information on how the strong interaction evolves from perturbative Quantum Chromodynamics (QCD) toward the non-perturbative regime where nucleon resonances (N^*) of different quantum numbers are generated from elementary quarks and gauge gluons. At the typical energy and distance scales found within the N^* states, the quark-gluon coupling is large. Therefore, we are confronted with the fact that quark-gluon confinement, hadron mass generation, and the dynamics that give rise to the N^* spectrum, cannot be understood within the framework of perturbative QCD. The need to understand QCD in this non-perturbative domain is a fundamental issue in nuclear physics, which the study of the spectrum and structure of N^* states can help to address. Such studies, in fact, represent a necessary step toward understanding how QCD in the regime of large quark-gluon couplings generates mass and how systems of confined quarks and gluons, i.e. mesons and baryons, are formed.

Electroproduction reactions $\gamma^* N \rightarrow N^* \rightarrow M + B$ provide a tool to probe the inner structure of the contributing N^* resonances through the extraction of the amplitudes for the transition between the virtual photon-nucleon initial state and the intermediate excited N^* state, i.e. the $\gamma_v N N^*$ electrocoupling amplitudes, which are directly related to the N^* structure. These electrocouplings can be represented by the so-called helicity amplitudes $A_{1/2}(Q^2)$ and $A_{3/2}(Q^2)$ that describe N^* resonance electroexcitation for the two different helicity configurations of a transverse photon and a nucleon, and $S_{1/2}(Q^2)$ that describes the N^* resonance electroexcitation by longitudinal photons of zero helicity [3]. Detailed comparisons of the theoretical predictions for these amplitudes with their experimental measurements form the basis of progress toward testing our understanding of non-perturbative QCD.

The studies of low-lying excited states of the nucleon using electromagnetic probes at four-momentum transfers $Q^2 < 5$ GeV^2 have revealed that the structure of these N^* states is a complex interplay between the internal core of three dressed quarks and an external meson-baryon cloud. Fig. 1 illustrates the two contributions to the $\gamma_v N N^*$ electrocouplings. In Fig. 1(b) the virtual photon interacts directly with the constituent quark, an interaction that is sensitive to the quark current and depends on the quark-mass function. However, the full meson electroproduction amplitude in Fig. 1(a) requires contributions to the $\gamma_v N N^*$ vertex from both non-resonant meson electroproduction and the hadronic scattering amplitudes as shown in Fig. 1(c). These contributions incorporate all possible intermediate meson-baryon states and all possible meson-baryon scattering processes that eventually result in the N^* formation in the intermediate state of the reaction. These two contributions have been separated from each another using, for example, a coupled-channel reaction model [4]. N^* states of different quantum numbers have significantly different relative contributions from these two components, demonstrating distinctly different manifestations of the non-perturbative strong interaction in their generation. The relative contribution of the quark

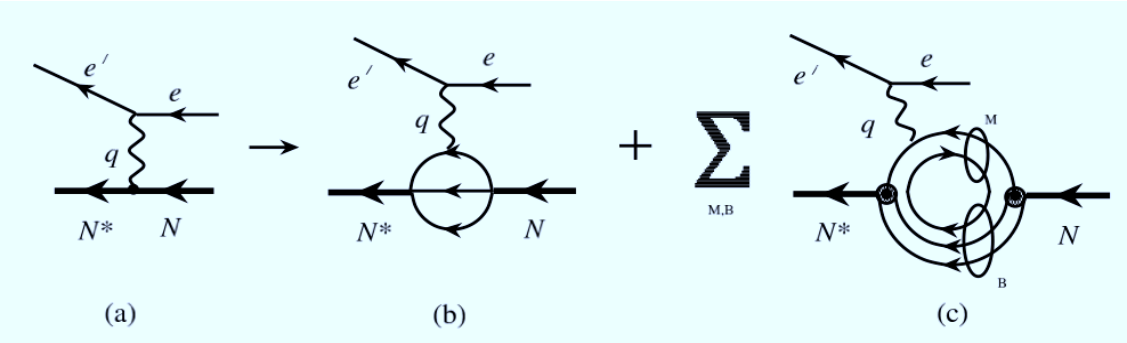

Figure 1: Schematic representation of the $\gamma^* N \to N^*$ electroproduction process [5]. (a) The fully dressed $\gamma_v N N^*$ electrocoupling that determines the N^* contribution to the resonant part of the meson electroproduction amplitude. (b) The contribution of the three-quark core. (c) The contribution from the meson-baryon cloud, where the sum runs over all intermediate meson and baryon states.

core increases with Q^2 in a gradual transition to a dominance of quark degrees of freedom for $Q^2 > 5$ GeV^2. This kinematics area still remains almost unexplored in exclusive reactions. Studies of the Q^2 evolution of N^* structure from low to high Q^2 offer access to the strong interaction between dressed quarks in the non-perturbative regime that is responsible for N^* formation. Mapping the Q^2 evolution of the structure of N^* states is an important aspect of the N^* program in Hall B, with both the existing completed experiments with CLAS and the future planned experiments with CLAS12.

Two dedicated experiments on studies of the spectrum and structure of N^* states in exclusive meson electroproduction off the proton with the CLAS12 detector have already been approved to run during the first physics running period with CLAS12. E12-09-003 [6] will measure the differential cross sections for exclusive non-strange meson (πN, ηN) and double-pion electroproduction. E12-06-108A [7] will measure differential cross sections and separated structure functions for the strangeness channels with primary focus on the $K^+\Lambda$ and $K^+\Sigma^0$ final states. These two experiments will acquire data at a beam energy of 11 GeV and probe Q^2 in the region from 5 GeV^2 to 12 GeV^2, the highest photon virtualities ever probed in these exclusive final states. From these cross section measurements, the electromagnetic transition form factors for all well-established N^* states for W up to 3 GeV for 5 GeV^2 $< Q^2 <$ 12 GeV^2 will be extracted. This new proposal to study the KY final states at lower beam energies of 6.6 GeV and 8.8 GeV will allow for precision data that fully overlap the existing lower Q^2 data acquired from CLAS and the higher Q^2 data from E12-06-108A. Together these experiments will allow for measurements of precision experimental observables and structure information over an unprecedented range of Q^2 from 2 GeV^2 to 12 GeV^2.

Recent advances in the Dyson-Schwinger equations (DSE) of QCD [8, 9] have demonstrated that the external meson-baryon structure generated by confined dressed quarks in the regime of dynamical chiral symmetry breaking (DCSB) should be substantial. The proposed experiment will cover the transition between large distances where there are essential contributions from both the meson-baryon cloud and the quark core, and small distances where the quark core is expected to dominate. Therefore the proposed experiment will address for the first time the challenging issue in hadron physics as to how the external meson-baryon cloud in the structure of N^* states is generated by the quarks and gluons confined in the inner

quark core. The DSE framework also provides an important link between the phenomenology of dressed current quarks and Lattice QCD (LQCD) [5]. Relations between baryon form factors and the Generalized Parton Distributions (GPDs) have also been developed that connect these two different approaches for describing baryon structure [10, 11].

Measurements of the $\gamma_v NN^*$ electrocouplings from low to high photon virtualities are needed in order to gain access to the dynamical momentum-dependent mass and structure of the dressed quark in the non-perturbative domain where the quark-gluon coupling is large [12], through mapping of the dressed quark mass function [13] and extractions of the quark distribution amplitudes for N^* states of different quantum numbers [14]. This is critical in exploring the nature of quark-gluon confinement and DCSB in baryons. Fig. 2 shows that the quark mass function $M(p)$ approaches a current quark mass of several MeV only in the high-momentum region of perturbative QCD. As the momentum p decreases, the current quark is dressed by gluons and acquires its usual constituent mass of ∼300 MeV. This result was initially predicted by DSE calculations and subsequently confirmed by LQCD [5]. Experimental verification of this momentum dependence would further improve our understanding of the dynamics of non-perturbative QCD. Efforts are underway [15] to study the sensitivity of transition form factors to different parameterizations of the momentum dependence of the quark mass.

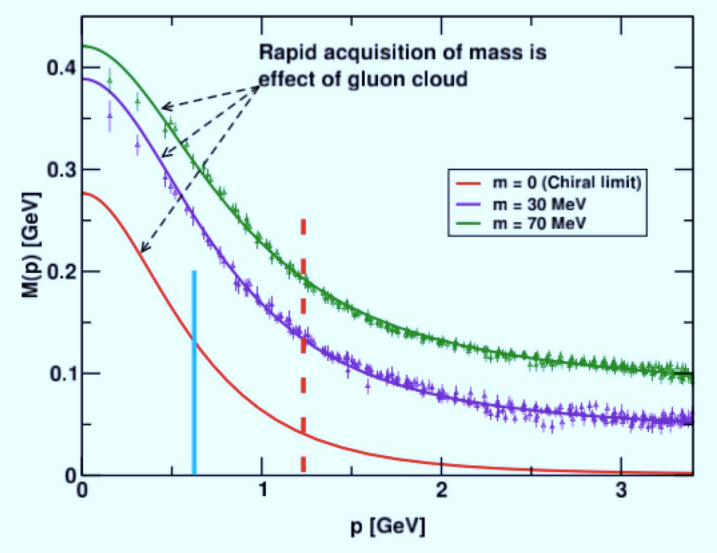

Figure 2: The momentum dependence of the quark mass [5]. The solid circles with error bars are from LQCD calculations with different lattice spacings characterized by the pion mass m as indicated in the key. The curves are from DSE calculations. The momentum regions that are accessible from the studies with beam energies of 6 GeV and 11 GeV are shown to the left of the blue vertical line and the red dashed line, respectively.

The invariant mass range of focus for the KY experiments, 1.6 GeV $< W <$ 3 GeV, is precisely the mass range where our knowledge of the N^* spectrum and the structure of these excited states is the most limited. While the field has slowly and methodically been making progress toward a better understanding of the low-lying N^* states in the region below 1.6 GeV, the host of the predicted missing N^* and Δ^* states lie in the region from 1.6 GeV $< W <$ 3 GeV. Figs. 3 and 4 show the N^* and Δ^* spectra predicted using the Bonn relativistically covariant quark model [16]. Fig. 5 shows the baryon spectrum from a recent

LQCD calculation [17] that shows very good correspondence with the calculations from the quark model. These figures highlight that detailed studies of the mass region provided by the KY final states will be essential to come to a more complete understanding of the structure of the states in the nucleon spectrum. Studies of the structure of the N^* states from low to high Q^2 may prove particularly valuable in this regard due to the fact that the ratio of the resonant N^* to the non-resonant background contributions is expected to improve with increasing photon virtuality. As such, we can hope to provide improved information on the poorly known higher-lying N^* states.

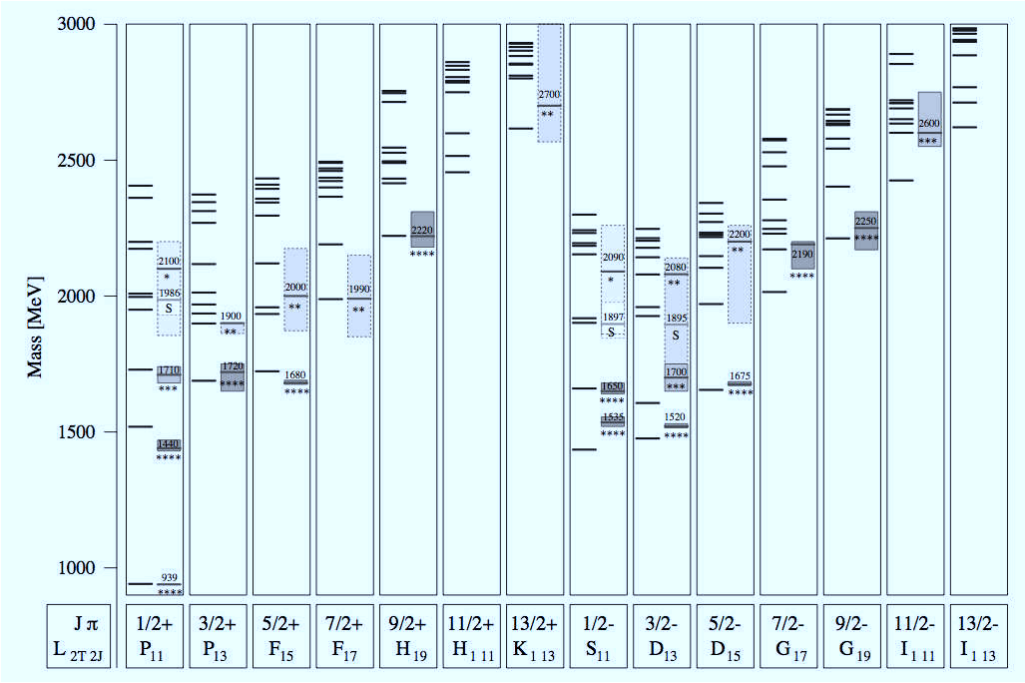

Figure 3: The N^* spectrum from the Bonn relativistically covariant quark model [16]. The known PDG states [18] are listed in the boxes on the right-hand side of each column.

Reliable information on KY hadronic decays from N^*s is not yet available. However, the N^* electrocoupling amplitudes can be obtained from fits to the extensive existing CLAS KY electroproduction data over the range 0.5 GeV^2 $< Q^2 <$ 4 GeV^2 (see Section 2.2), which should be carried out independently in different bins of Q^2, utilizing the Q^2-independent behavior of resonance hadronic decays. A successful description of the exclusive KY electroproduction data with the same KY partial hadronic decay widths in all measured Q^2 bins will improve the information on the poorly known KY decays of nucleon resonances. The development of reaction models for the extraction of the $\gamma_v NN^*$ electrocouplings from the KY electroproduction channels is urgently needed. The work to extract the amplitudes for the prominent N^* and Δ^* states that couple to the strangeness channels $K^+\Lambda$ and $K^+\Sigma^0$ is now getting underway for the CLAS data acquired for $Q^2 <$ 4 GeV^2.

Under the aegis of the existing CLAS12 N^* program (E12-09-003 and E12-06-108A), a strong collaboration between experimentalists and theorists has been brought together to achieve the challenging objectives in pursuing N^* studies from low to high Q^2 [5, 6, 7]. This new proposal to study the $N^* \to KY$ exclusive channels has been developed as an important extension of the existing CLAS12 N^* program. The main goals of this new effort are i) to provide the KY electroproduction cross sections and polarization observables needed for the

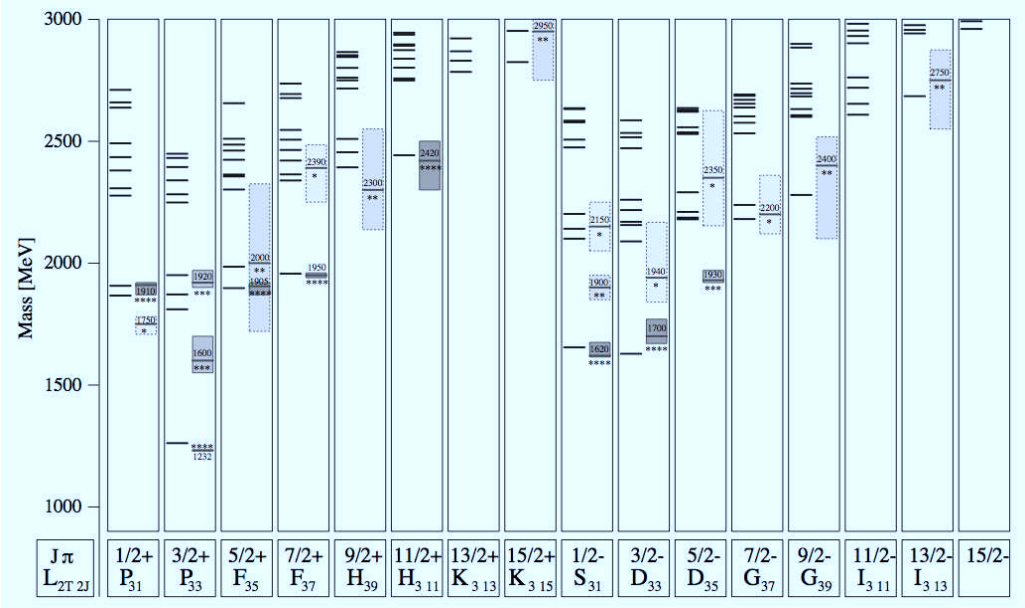

Figure 4: The Δ^* spectrum from the Bonn relativistically covariant quark model [16]. The known PDG states [18] are listed in the boxes on the right-hand side of each column.

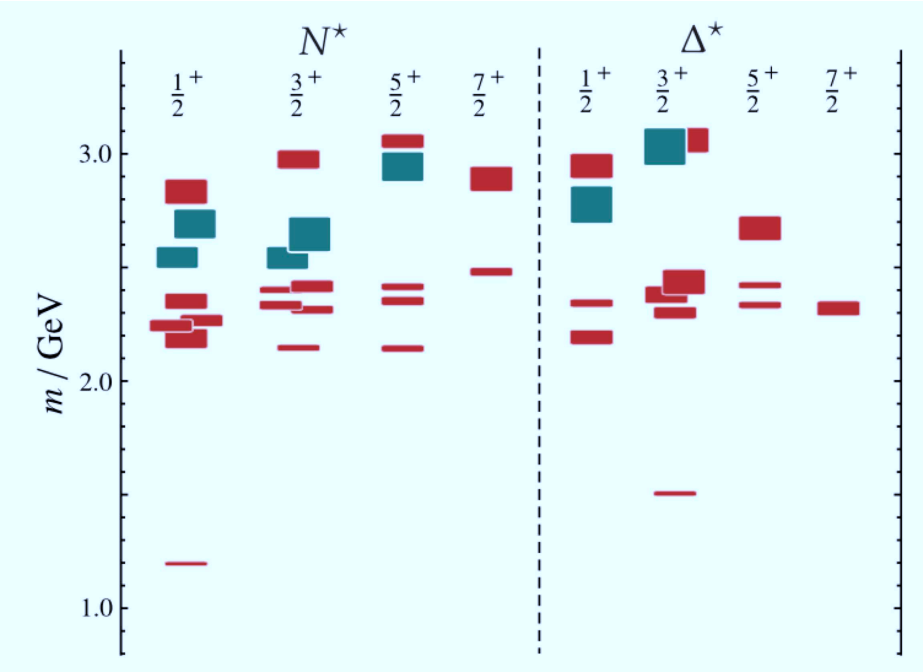

Figure 5: The baryon spectrum derived from LQCD calculations [17] with m_π=391 MeV. The states shown in red represent conventional qqq states while those in blue represent hybrid states featuring a gluonic excitation.

development of the reaction models to extract the $\gamma_v NN^*$ electrocouplings that incorporate the transition from meson-baryon to quark degrees of freedom into the reaction mechanisms and ii) to develop approaches for the theoretical interpretation of the $\gamma_v NN^*$ electrocouplings that are capable of exploring how N^* states of different quantum numbers are generated non-perturbatively by the strong interaction in processes that emerge from QCD.

In the last decade there has been marked progress in developing more realistic and more complete theoretical approaches. CQMs have been greatly refined by using fully relativistic treatments [19, 20, 21, 22] and by including sea quark components [23], and hypercentric CQMs with more proper treatment of constituent quark interactions have been developed [24, 25]. In addition, a covariant model based on the Dyson-Schwinger equations of QCD [8, 9, 26, 27, 28, 29, 30] has been shown to allow the baryon data to be interpreted starting from the QCD Lagrangian.

Recently, a successful description of the data on nucleon elastic and transition $N \rightarrow \Delta(1232)\frac{3}{2}^-$ and $N \rightarrow N(1440)\frac{1}{2}^+$ form factors was achieved with the same momentum dependence of the dressed quark mass [12, 31]. A successful description of the elastic and transition form factors for electroexcitation of N^* states of distinctly different structure conclusively demonstrated the relevance of dressed quarks as the effective degree of freedom in the structure of the ground and excited nucleons, and the possibility to explore this fundamental ingredient of the non-perturbative strong interaction from the data on elastic and transition $N \rightarrow N^*$ form factors. This success emphasizes the importance of this proposed experiment as an essential part of the efforts to address the most challenging open problems of the Standard Model on the nature of >98% of hadron mass and quark-gluon confinement. On a fundamental level, LQCD is progressing rapidly toward making direct contact with the baryon data. Toward this end, the USQCD Collaboration [32] (which involves JLab's LQCD group) is working to perform calculations for predicting the baryon spectrum, as well as the $\gamma_v NN^*$ transition form factors.

In the past decade the Excited Baryon Analysis Center (EBAC) at JLab made significant contributions to develop rigorous approaches to not only extract the N^* parameters from the available data, but also to develop a complete framework with which to interpret these data in terms of QCD-based approaches (CQMs, DSE, LQCD). A summary of the EBAC program (completed in 2012) is detailed in Ref. [5]. Further progress is expected due to continuing developments on amplitude analysis at the JLab Physics Analysis Center [33]. Finally, the important work undertaken by the EBAC effort is being extended by the Argonne-Osaka Collaboration [4], whose goal is to extend the analysis of meson production amplitudes through their dynamical coupled-channel approach to extract the mass, width, hadronic coupling constants, and electromagnetic transition form factors of the N^* states across the full resonance region. Ultimately the results on the resonance parameters from analysis of the full set of expected meson electroproduction data from CLAS12 will allow access to the dynamics of the non-perturbative strong interaction responsible for N^* formation. These analyses will be crucial for understanding the nature of confinement and dynamical chiral symmetry breaking in baryons.

2 CLAS N^* Program

Studies of the spectrum and structure of excited nucleon states, the so-called N^* program, is one of the key cornerstones of the physics program in Hall B. The large acceptance spectrometer CLAS [34], which began data taking in 1997 and was decommissioned in 2012, was designed to measure photo- and electroproduction cross sections and polarization observables for beam energies up to 6 GeV over a broad kinematic range for a host of different exclusive reaction channels. Consistent determination of N^* properties from different exclusive channels with different couplings and non-resonant backgrounds offers model-independent support for the findings.

To date photoproduction datasets from CLAS and elsewhere have been used extensively to constrain coupled-channel fits and advanced single-channel models. However, data at Q^2=0 allows us to identify N^* states and determine their quantum numbers, but tell us very little about their structure. It is the Q^2 dependence of the $\gamma_v NN^*$ electrocouplings that unravels and reveals these details. In addition, electrocoupling data are promising for studies of nucleon excited states as the ratio of resonant to non-resonant amplitudes increases with increasing Q^2. Finally, the electroproduction data are an effective tool to confirm the existence of new N^* states as the data must be described by Q^2-independent resonance masses and hadronic decay widths.

The goal of the N^* program with CLAS is to study the spectrum of N^* states and their associated structure over a broad range of distance scales through studies of the Q^2 dependence of the $\gamma_v NN^*$ electrocouplings. For each final state this goal is realized through two distinct phases. The first phase consists of the measurements of the cross sections and polarization observables in as fine a binning in the relevant kinematic variables Q^2, W, $d\tau_{hadrons}$ (where $d\tau_{hadrons}$ represents the phase space of the final state hadrons) as the data support. The second phase consists of developing advanced reaction models that describe the data over its full phase space in order to then extract the electrocoupling amplitudes for the prominent contributing N^* states.

2.1 Non-Strange Final States

Electrocoupling amplitudes for most N^* states below 1.8 GeV have been extracted for the first time from analysis of CLAS data for the exclusive $\pi^+ n$ and $\pi^0 p$ channels for Q^2 up to 5 GeV^2, for ηp for Q^2 up to 4 GeV^2, and for $\pi^+\pi^- p$ for Q^2 up to 1.5 GeV^2. Fig. 6 shows representative CLAS data for the $A_{1/2}$ electrocouplings for the $N(1440)\frac{1}{2}^+$, $N(1520)\frac{3}{2}^-$, and $N(1675)\frac{5}{2}^-$ [5, 35, 36, 37]. Studies of the electrocouplings for N^* states of different quantum numbers at lower Q^2 have revealed a very different interplay between the inner quark core and the meson-baryon cloud as a function of Q^2. Structure studies of the low-lying N^* states, e.g. $\Delta(1232)\frac{3}{2}^+$, $N(1440)\frac{1}{2}^+$, $N(1520)\frac{3}{2}^-$, and $N(1535)\frac{1}{2}^-$, have made significant progress in recent years due to the agreement of results from independent analyses of the CLAS πN and $\pi\pi N$ final states [5, 35, 37, 38, 39, 40]. The good agreement of the extracted electrocouplings from both the πN and $\pi\pi N$ exclusive channels is non-trivial in that these channels have very different mechanisms for the non-resonant backgrounds. The agreement thus provides compelling evidence for the reliability of the results.

The size of the meson-baryon dressing amplitudes are maximal for $Q^2 < 1$ GeV^2 (see

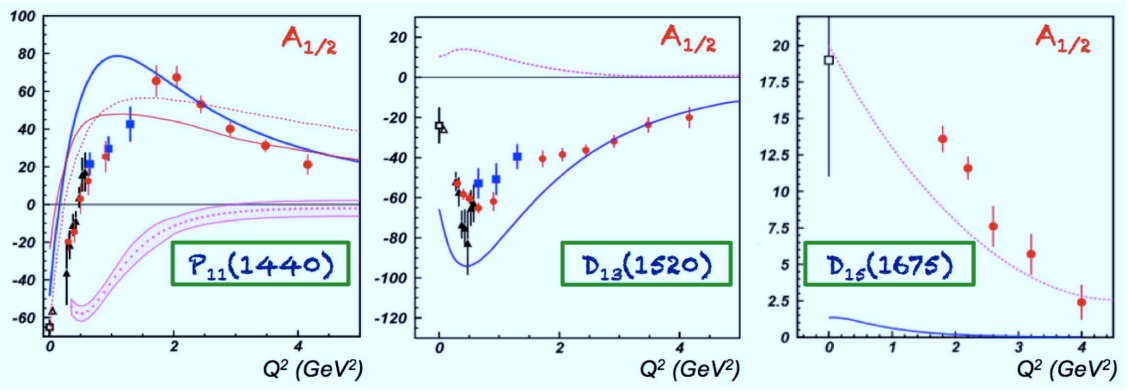

Figure 6: The $A_{1/2}$ electrocoupling amplitudes (in units of 10^{-3} GeV$^{-1/2}$) vs. Q^2 (GeV^2) for the N^* states $N(1440)\frac{1}{2}^+$ (left), $N(1520)\frac{3}{2}^-$ (middle), and $N(1675)\frac{5}{2}^-$ (right) from analyses of the CLAS πN (circles) and $\pi\pi N$ (triangles, squares) data. (Left) Calculation from a non-relativistic light-front quark model with a running quark mass (red line) and calculation of the quark core from the DSE approach (blue line). (Middle/Right) Calculations from the hypercentral constituent quark model (blue lines). The magnitude of the meson-baryon cloud contributions is shown by the magenta line (or band) on each plot. See Refs. [5, 35, 36, 37] for details on the data and the models.

Fig. 6). For increasing Q^2, there is a gradual transition to the domain where the quark degrees of freedom begin to dominate, as seen by the improved description of the N^* electrocouplings obtained within the DSE approach, which accounts only for the quark core contributions. For $Q^2 > 5$ GeV^2, the quark degrees of freedom are expected to fully dominate the N^* states [5]. Therefore, the $\gamma_v NN^*$ electrocoupling amplitudes extracted from these data at beam energies of 6.6 GeV and 8.8 GeV will probe N^* structure in the low Q^2 domain where meson-baryon degrees of freedom dominate and the high Q^2 domain where the quark core dynamics dominate.

Analysis of CLAS data for the $\pi\pi N$ channel has provided the only detailed structure information available regarding higher-lying N^* states, e.g. $\Delta(1620)\frac{1}{2}^-$, $N(1650)\frac{1}{2}^-$, $\Delta(1700)\frac{3}{2}^-$, and $N(1720)\frac{3}{2}^+$. Fig. 7 shows a representative set of illustrative examples for $S_{1/2}$ for the $\Delta(1620)\frac{1}{2}^-$ [37], as well as for $A_{1/2}$ for the $\Delta(1700)\frac{3}{2}^-$ and $A_{3/2}$ for the $N(1720)\frac{3}{2}^+$ [36]. Here the analysis for each N^* state was carried out independently in different bins of W across the width of the resonance for Q^2 up to 1.5 GeV^2 with very good correspondence within each Q^2 bin. Note that most of the N^* states with masses above 1.6 GeV decay preferentially through the $\pi\pi N$ channel instead of the πN channel.

2.2 *KY* Final States

With a goal to have an independent determination of the electrocouplings for each N^* state from multiple exclusive reaction channels, a natural avenue to investigate the higher-lying N^* states is the strangeness channels $K^+\Lambda$ and $K^+\Sigma^0$. In fact, data from the KY channels are critical to provide an independent extraction of the electrocoupling amplitudes for the higher-lying N^* states. The CLAS program has yielded by far the most extensive measurements of KY electroproduction data ever measured across the nucleon resonance

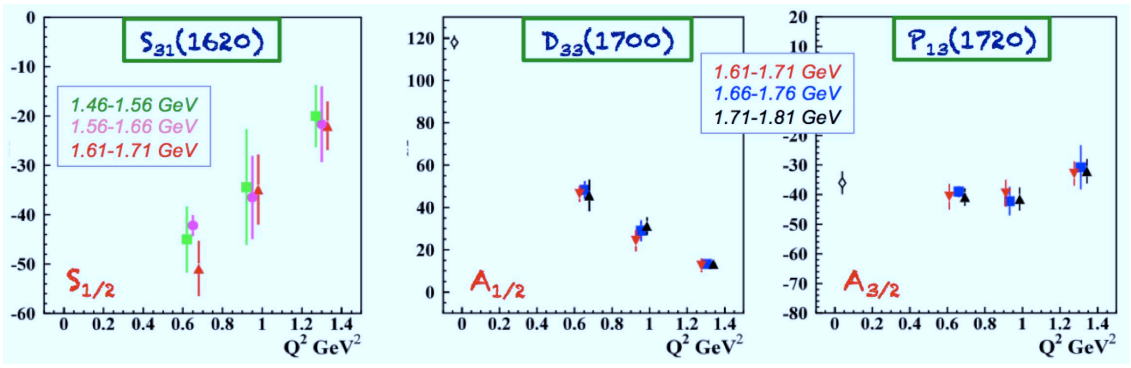

Figure 7: CLAS results for the N^* electrocoupling amplitudes (in units of 10^{-3} GeV$^{-1/2}$) from analysis of the exclusive $\pi^+\pi^- p$ final state as a function of Q^2 (GeV^2). (Left) $S_{1/2}$ of the $\Delta(1620)\frac{1}{2}^-$ [37], (middle) preliminary extraction of $A_{1/2}$ for the $\Delta(1700)\frac{3}{2}^-$ [36], and (right) preliminary extraction of $A_{3/2}$ for the $N(1720)\frac{3}{2}^+$ [36]. Each electrocoupling amplitude was extracted in independent fits in different bins of W across the resonance peak width as shown for each Q^2 bin (with the points at each Q^2 offset for clarity).

region. These measurements have included the differential cross sections and the separated structure functions σ_T, σ_L, $\sigma_U = \sigma_T + \epsilon\sigma_L$, σ_{LT}, σ_{TT}, and $\sigma_{LT'}$ for $K^+\Lambda$ and $K^+\Sigma^0$ [41, 42, 43, 44], the recoil polarization for $K^+\Lambda$ [45], and the beam-recoil transferred polarization for $K^+\Lambda$ and $K^+\Sigma^0$ [46, 47]. These measurements span Q^2 from 0.5 GeV^2 to 4.5 GeV^2, W from 1.6 GeV to 3.0 GeV, and the full center-of-mass angular range of the K^+.

Due to the creation of an $s\bar{s}$ quark pair in the intermediate state, the KY final states are naturally sensitive to coupling to higher-lying s-channel resonance states at $W > 1.6$ GeV, a region where our knowledge of the N^* spectrum is the most limited. Note also that although the two ground-state hyperons have the same valence quark structure (uds), they differ in isospin, such that intermediate N^* resonances can decay strongly to $K^+\Lambda$ final states, but intermediate Δ^* states cannot. Because $K^+\Sigma^0$ final states can have contributions from both N^* and Δ^* states, the hyperon final state selection constitutes an isospin filter. Shown in Figs. 8 and 9 is a small sample of the available data in the form of the $K^+\Lambda$ and $K^+\Sigma^0$ structure functions σ_U, σ_{LT}, σ_{TT}, and $\sigma_{LT'}$ [44, 48], illustrating the broad kinematic coverage and statistical precision of the data.

Figures 8 and 9 include two of the more advanced single channel reaction models for the electromagnetic production of KY final states. The MX model is the isobar model from Maxwell [49], and the RPR-2007 [50] and RPR-2011 [51] models are from the Ghent Regge plus Resonance (RPR) framework. Both the MX and RPR models were developed based on fits to the extensive and precise photoproduction data from CLAS and elsewhere and describe those data reasonably well. However, they fail to adequately describe the electroproduction data in any of the kinematic phase space. Reliable information on KY hadronic decays from N^*s is not yet available due to the lack of an adequate reaction model. However, after such a model is developed, the N^* electrocoupling amplitudes for states that couple to KY can be obtained from fits to the extensive existing CLAS KY electroproduction data over the range 0.5 GeV$^2 < Q^2 <$ 4.5 GeV^2, which should be carried out independently in different bins of Q^2 with the same KY hadronic decays, extending the available information on these N^* states and testing the consistency of the analysis. The development of such reaction models for

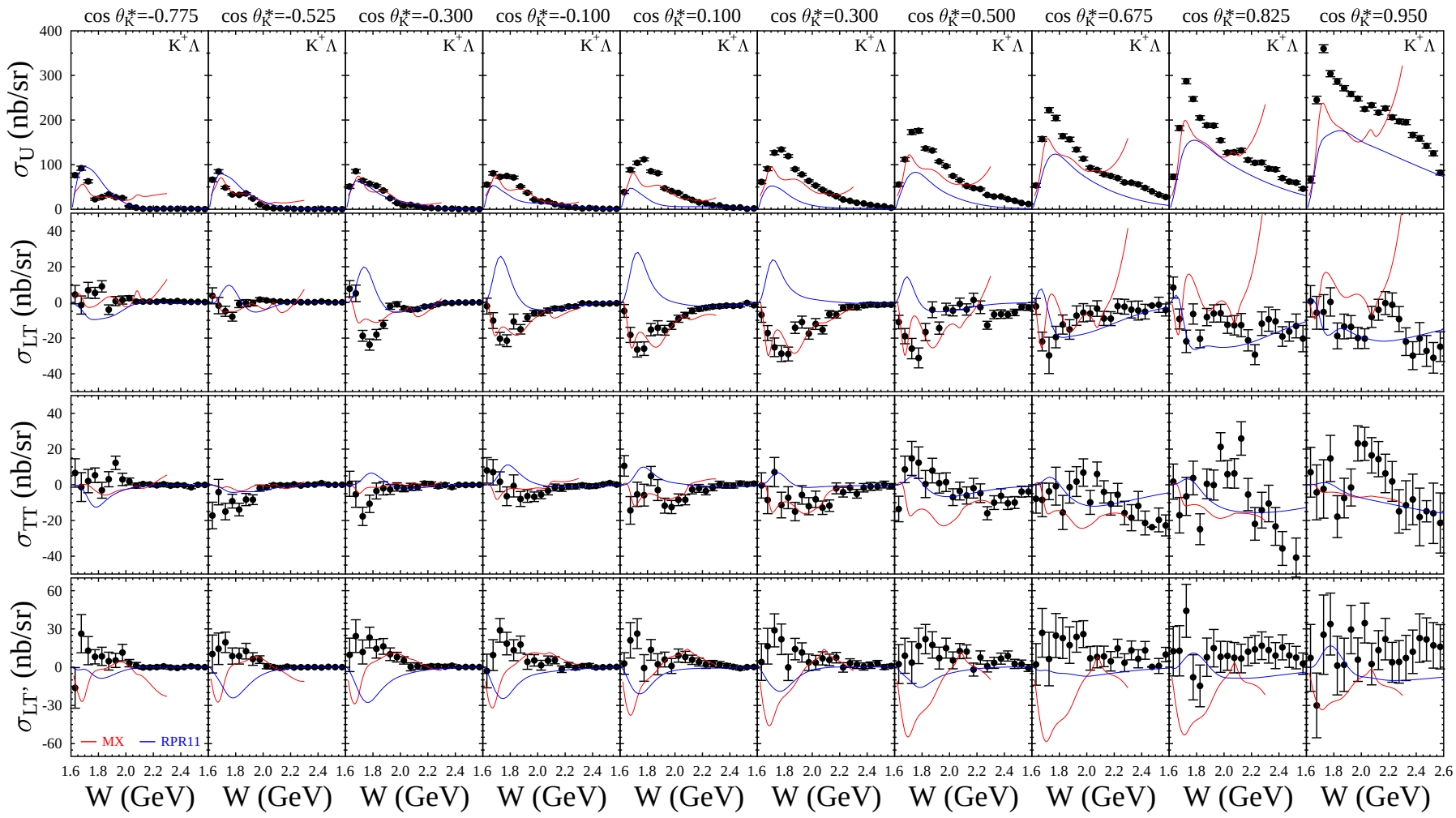

Figure 8: Structure functions $\sigma_U = \sigma_T + \epsilon\sigma_L$, σ_{LT}, σ_{TT}, and $\sigma_{LT'}$ (nb/sr) for $K^+\Lambda$ production vs. W (GeV) for E_b=5.5 GeV for Q^2=1.80 GeV^2 and $\cos\theta^*_K$ values as shown from CLAS data [44, 48]. The error bars represent the statistical uncertainties only. The red curves are from the hadrodynamic KY model of Maxwell [49] and the blue curves are from the hybrid RPR-2011 KY model from Ghent [51].

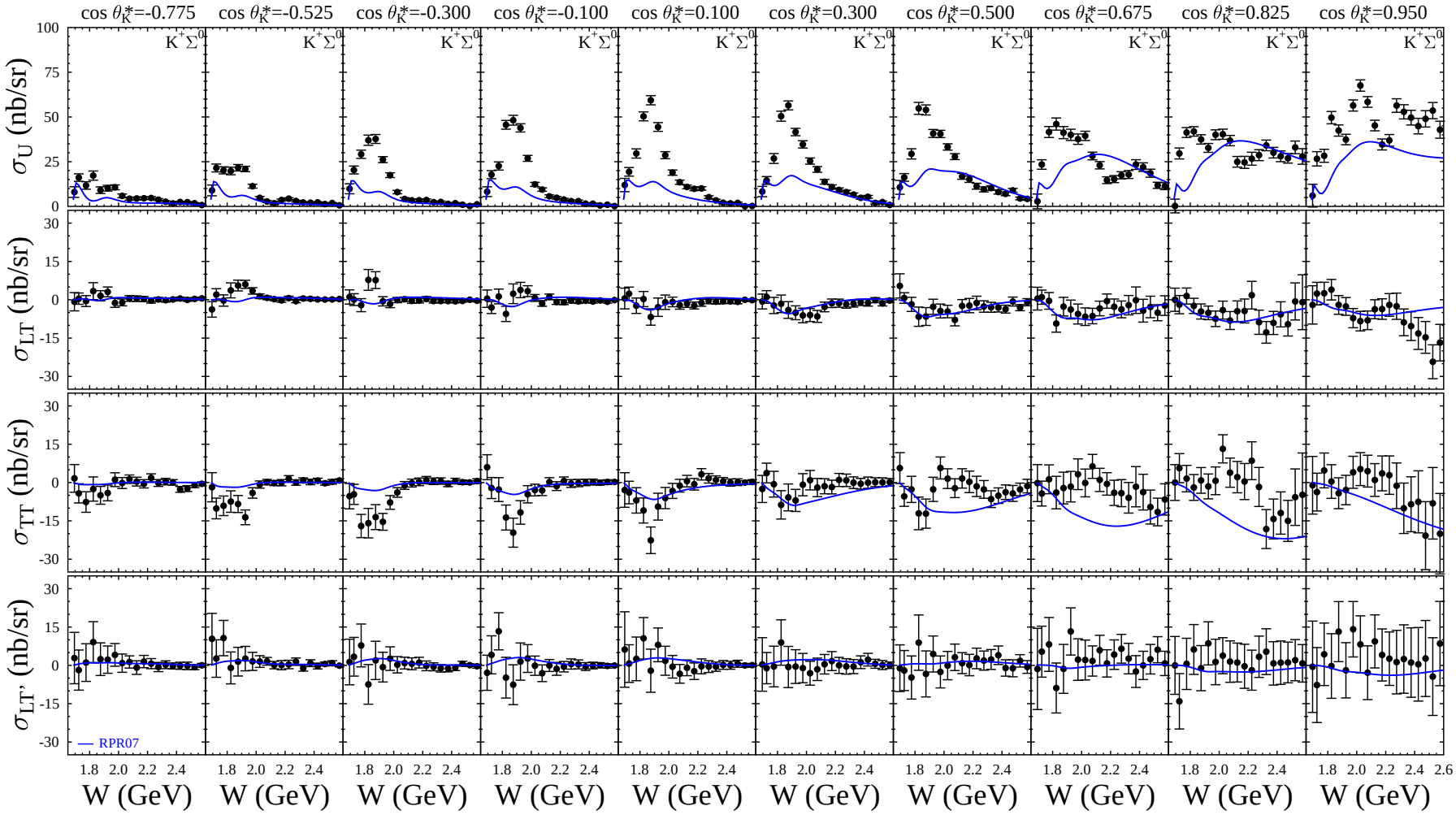

Figure 9: Structure functions $\sigma_U = \sigma_T + \epsilon\sigma_L$, σ_{LT}, σ_{TT}, and $\sigma_{LT'}$ (nb/sr) for $K^+\Sigma^0$ production vs. W (GeV) for E_b=5.5 GeV for Q^2=1.80 GeV^2 and $\cos\theta^*_K$ values as shown from CLAS data [44, 48]. The error bars represent the statistical uncertainties only. The blue curves are from the hybrid RPR-2007 KY model from Ghent [50].

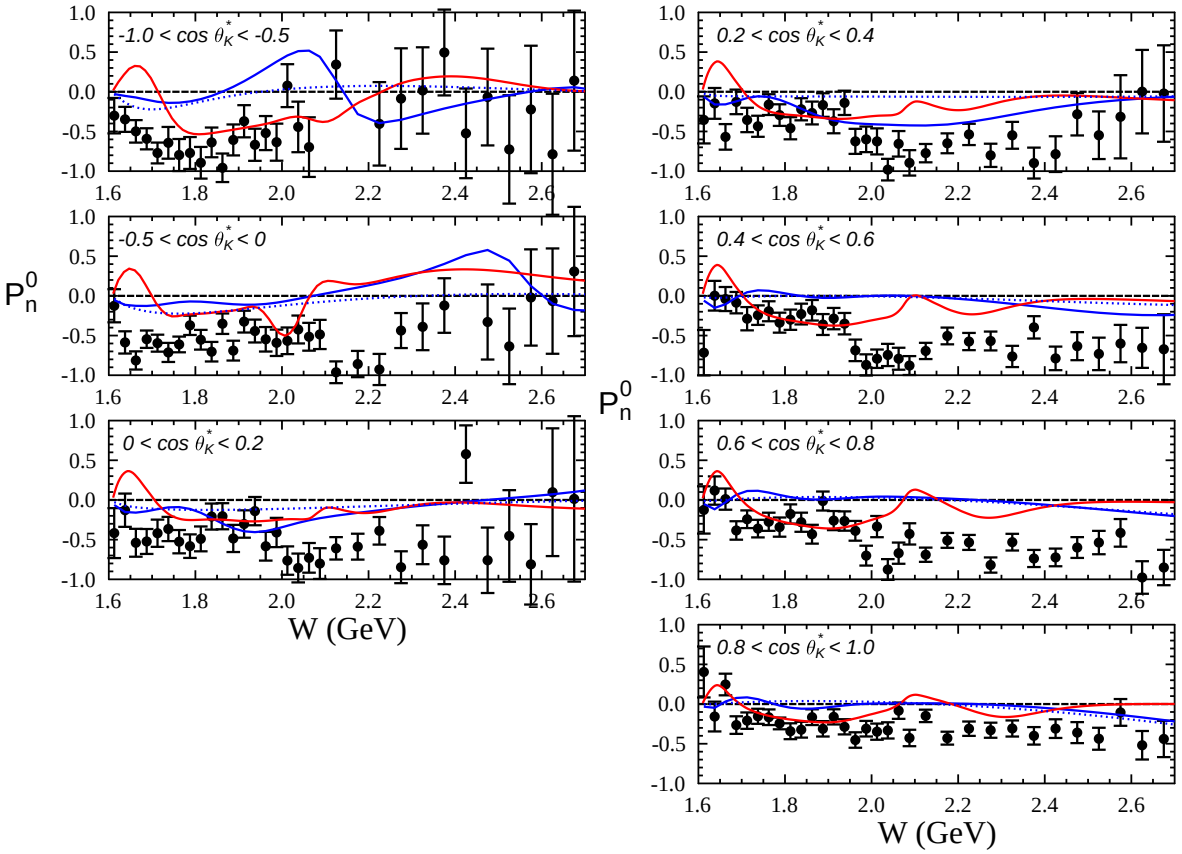

Figure 10: Induced polarization vs. W (GeV) for bins in $\cos\theta^*_K$ (as shown on the upper left of each plot) for an average $Q^2 = 1.9$ GeV^2 from CLAS $K^+\Lambda$ data [45]. The red curves are from the hadrodynamic KY model of Maxwell [49] and the blue curves are from the hybrid RPR-2011 KY model from Ghent [51].

the extraction of the $\gamma_v NN^*$ electrocouplings from the KY electroproduction channels has been initiated. A key element to the development of the reaction models for $K^+\Lambda$ and $K^+\Sigma^0$ production is the inclusion of constraints provided by the hyperon polarization observables. Fig. 10 shows the $K^+\Lambda$ induced polarization data from CLAS [45] and Fig. 11 shows the $K^+\Lambda$ beam-recoil transferred polarization data from CLAS. These data are overlaid with the predictions from the MX [49] and RPR [51, 50] models and show that they provide important constraints for the resonant and non-resonant diagrams in the models even with their relatively modest statistical precision.

To date the PDG [18] lists only four N^* states, $N(1650)\frac{1}{2}^-$, $N(1710)\frac{1}{2}^+$, $N(1720)\frac{3}{2}^+$, and $N(1900)\frac{3}{2}^+$, with known couplings to $K\Lambda$ and no N^* states are listed that couple to $K\Sigma$; only a single Δ^* state, $\Delta(1920)\frac{3}{2}^+$, is listed with coupling strength to $K\Sigma$. The branching ratios to KY provided for these states are less than 10% with uncertainties of the size of the measured coupling. While the relevance of this core set of N^* states in the $\gamma^{(*)}p \to K^+\Lambda$ reaction has long been considered a well-established fact, this set of states falls short of reproducing the experimental results for $W < 2$ GeV. A recent development in understanding the N^* spectrum was provided by the Bonn-Gatchina coupled-channel partial wave analysis of the final state reactions produced through the $N\pi$ and γp reactions [52]. This work presents an

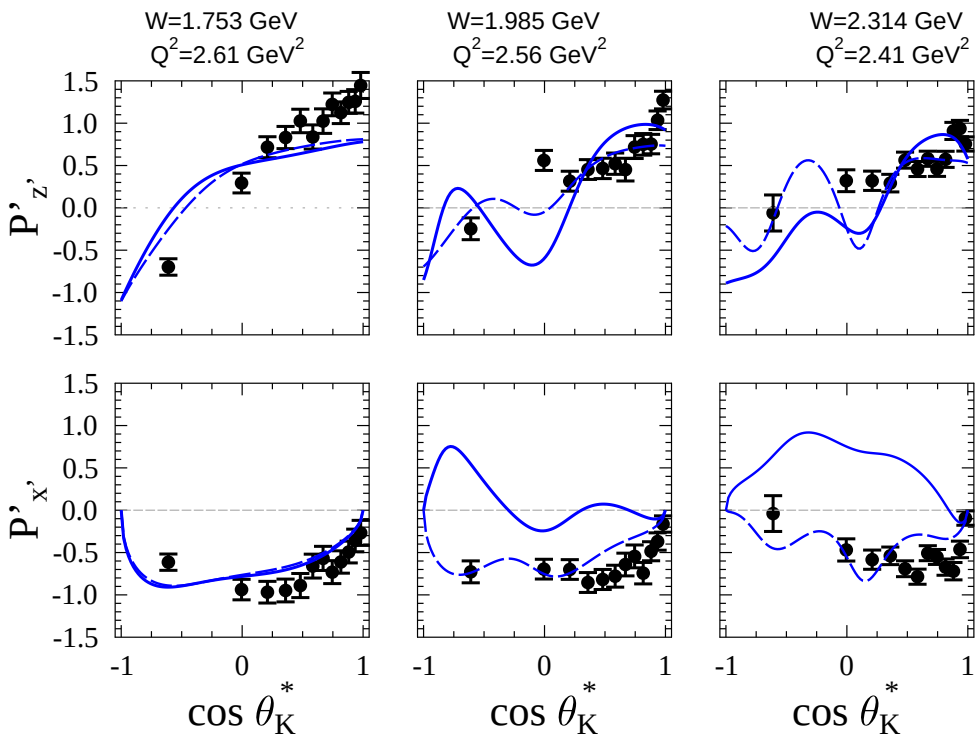

Figure 11: Beam-recoil transferred polarization data vs. $\cos\theta^*_K$ for representative bins in W and Q^2 from CLAS $K^+\Lambda$ data [47]. The curves are variants of the RPR-2007 model [50] including different N^* states at 1.9 GeV (dashed - D_{13}, solid - P_{11}).

up-to-date listing of pole parameters and branching fractions for all N^* and Δ^* states up to $\sim$2 GeV with uncertainties at the level of a few percent. That analysis provided a list of six N^* states with coupling to $K\Lambda$, five N^* states with coupling to $K\Sigma$, and four Δ^* states with coupling to $K\Sigma$. For more on this list of states that couple to $K\Lambda$ and $K\Sigma$, see Ref. [53].

The findings of Ref. [52] are based on a significant amount of precision experimental data and a sophisticated coupled-channel fitting algorithm. However, in general, the issue of how to extract N^* content from open strangeness reactions is a long-standing question. Various analyses have led to very different conclusions concerning the set of resonances that contribute (e.g. compare results from Refs. [54, 55, 56], as well as the statements made regarding the resonant set from Ref. [52]). Furthermore, lack of sufficient experimental information, incomplete kinematic coverage, and underestimated systematics are still responsible for inconsistencies among the different models that fit the data to extract the contributing resonances and their properties [56, 57]. The availability of precision electroproduction data to include in the fitting database to constrain the coupled-channel fits is expected to reduce the solution ambiguities and the algorithm dependence of the results.

3 CLAS12 N^* Program Objectives

The full experimental program of N^* studies with the CLAS12 detector has a number of important objectives. These include:

i) To map out the quark structure of the dominant N^* and Δ^* states from the data

acquired for meson electroproduction through the exclusive final states including $p\pi^0$, $n\pi^+$, $p\eta$, $p\omega$, $p\pi^+\pi^-$, $K^+\Lambda$, and $K^+\Sigma^0$. This objective is motivated by results from existing analyses such as those shown in Fig. 6, where it is seen that the meson-baryon dressing contribution to the N^* structure decreases rapidly with increasing Q^2. The data can be described approximately in terms of dressed quarks already for $Q^2 \sim 5$ GeV^2. It is therefore expected that data that span from low to high Q^2 can map out the transition from the regime where low-energy degrees of freedom dominate to the regime where the quark core fully dominates the dynamics of the N^* and Δ^* states. The comparison of the extracted resonance electrocoupling parameters over this broad Q^2 regime to the predictions from LQCD and DSE calculations will allow for a much improved understanding of how the internal dressed quark core emerges from QCD and how the dynamics of the strong interaction are responsible for the formation of the N^* and Δ^* states of different quantum numbers.

ii) To investigate the dynamics of dressed quark interactions and how they emerge from QCD. This work is motivated by recent developments of hadronic models based on the DSE approach, and has provided links between the dressed quark propagator, the dressed quark scattering amplitudes, and the QCD Lagrangian. DSE analyses of the extracted N^* electrocoupling parameters have the potential to allow for investigation of the origin of dressed quark confinement in baryons and the nature of DCSB, since both of these phenomena are rigorously incorporated into DSE approaches [5, 8, 9].

iii) To study the Q^2-dependence of the non-perturbative dynamics of QCD. This is motivated by studies of the momentum dependence of the dressed quark mass function of the quark propagator within LQCD [58] and DSE [26, 27]. The calculated mass function approaches the current quark mass of a few MeV only in the high Q^2 regime of perturbative QCD. However, for decreasing momenta, the current quark acquires a constituent mass of $\sim$300 MeV as it is dressed by quarks and gluons. Verification of this momentum dependence would further advance understanding of non-perturbative dynamics. Efforts are currently underway to study the sensitivity of the proposed transition form factor measurements to different parameterizations of the momentum dependence of the quark mass [59].

iv) To offer constraints from resonance transition form factors for the $N \rightarrow N^*$ GPDs. We note that a key aspect of the CLAS12 measurement program is the characterization of exclusive reactions at high Q^2 in terms of GPDs. The elastic and $\gamma_v NN^*$ transition form factors represent the first moments of the GPDs [15, 60, 61], and they provide for unique constraints on the structure of nucleons and their excited states. Thus the N^* program at high Q^2 represents the initial step in a reliable parameterization of the transition $N \rightarrow N^*$ GPDs and is an important part of the larger overall CLAS12 program studying exclusive reactions. The studies of the CLAS results on $\gamma_v NN^*$ electrocouplings for the $N(1535)\frac{1}{2}^-$ resonance within the Light Cone Sum Rule approach coupled to LQCD have already provided access for the first time to parton degrees of freedom in the N^* structure in terms of quark distribution amplitudes [62].

The proposed experiment will complement these objectives. For the first time in a single experiment we will scan the Q^2 range below 5 GeV^2 where the contributions from both the meson-baryon cloud and quark core are relevant and the Q^2 range above 5 GeV^2 where the quark core dominance is expected with the final states that require the creation of an $s\bar{s}$

pair. It offers a unique opportunity to explore the emergence of the external meson-baryon cloud from the core of confined quarks and gluons and to check the theoretical expectations on the meson-baryon cloud generation from the confinement regime.

4 Experiment Details

4.1 Experimental Overview

The CLAS12 spectrometer [63] is designed for operation at beam energies up to 11 GeV (the maximum possible for delivery to Hall B) and will operate at a nominal beam-target luminosity of 1×10^{35} cm^{-2}s^{-1}, an order of magnitude increase over previous CLAS operation. This luminosity will allow for precision measurements of cross sections and polarization observables for many exclusive reaction channels for invariant energies W up to 3 GeV, the full decay product phase space, and four-momentum transfers Q^2 up to 12 GeV^2. The physics program for CLAS12 focuses on measurements of the spatial and angular momentum structure of the nucleon, investigation of quark confinement and hadron mass generation in the spectrum and structure of the ground- and excited-state nucleons, and studies of the strong interaction in nuclei. The CLAS12 physics program currently consists of nine separate run groups. However, at the present time, there is no approved beam time for running at electron beam energies below 11 GeV.

We plan to measure the exclusive $K^+\Lambda$ and $K^+\Sigma^0$ final states from a liquid-hydrogen target with the CLAS12 spectrometer using a longitudinally polarized electron beam with the maximum possible polarization (>80%). The experiment will operate with the torus at the maximum possible current (assumed to be $B = 0.9B_{max}$ or I=3375 A) set with a polarity such that negatively charged particles bend away from the electron beamline. These parameters are fully consistent with those for the other experiments that are part of this new proposed run group. At incident beam energies of 6.6 GeV and 8.8 GeV, we will measure the differential cross sections and hyperon polarization components over a range of invariant energies 1.6 GeV $< W <$ 3 GeV in the domain of momentum transfers Q^2 from 2 GeV^2 to 7 GeV^2, while spanning the full center-of-mass angular range of the final state K^+. Measurements in the range of $Q^2 < 4$ GeV^2 will provide significant overlap to connect to the existing CLAS KY data from Refs. [41, 42, 43, 44, 45, 46, 47]. In fact, these data for $Q^2 < 4$ GeV^2 will actually well extend the observables already published from analysis of the CLAS electroproduction data highlighted in Section 2.2 in Figs. 8 to 11 due to the significant factor of increase in the expected statistics compared to the CLAS data of ∼10 at Q^2=4 GeV^2 and ∼100 at Q^2=2 GeV^2. The data in the range from Q^2=4 GeV^2 to 7 GeV^2 provides the bridge of new data to overlap with the high Q^2 data from E12-06-108A [7] that will take data at a beam energy of 11 GeV during the first CLAS12 physics running period scheduled to take data in 2017.

4.2 Stage 1 Analysis

The first stage of the analysis of the experimental data will be to extract the differential cross sections, the separated structure functions, and the induced and transferred polarizations

for the $K^+\Lambda$ and $K^+\Sigma^0$ final states. In this section the specific observables to be measured and the path to their extraction from the measured data are detailed.

Following the notation of Refs. [44, 47, 64], for the case of an unpolarized electron beam (helicity h=0) with no target or recoil polarizations, the virtual photon cross section for the K^+Y electroproduction reaction can be written (using simplifying notation for the differential cross section) as:

$$\frac{d\sigma}{d\Omega_K^*} \equiv \sigma_0 = \sigma_U + \epsilon\sigma_{TT}\cos 2\Phi + \sqrt{\epsilon(1+\epsilon)}\sigma_{LT}\cos\Phi, \tag{1}$$

where σ_i are the structure functions that measure the response of the hadronic system and $i = T$, L, LT, and TT represents the transverse, longitudinal, and interference structure functions. The structure functions are, in general, functions of Q^2, W, and θ_K^* only. The unseparated structure function is defined as $\sigma_U = \sigma_T + \epsilon\sigma_L$. Here Φ is the angle between the electron scattering plane and the KY hadronic reaction plane and ϵ is the virtual photon polarization parameter defined as:

$$\epsilon = \left(1 + 2\frac{\nu^2}{Q^2}\tan^2\frac{\theta_{e'}}{2}\right)^{-1}, \tag{2}$$

where $\theta_{e'}$ is the electron scattering angle in the laboratory frame and ν is the energy transfer of the virtual photon. Fig. 12 shows the kinematics for the KY electroproduction reaction in the γ^*-target proton center-of-mass (CM) frame and the coordinate system employed for the polarization formalism.

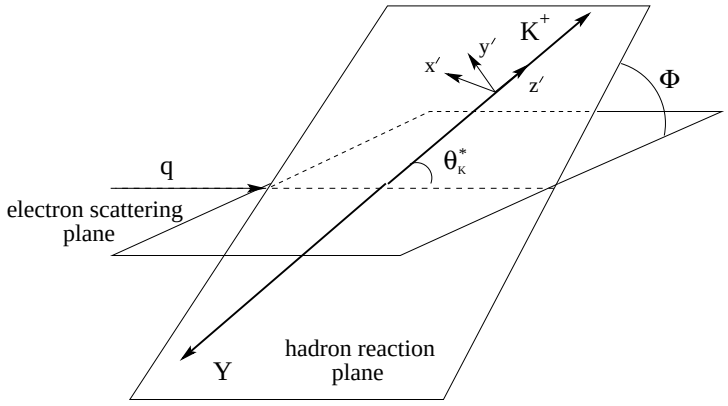

Figure 12: Kinematics for KY electroproduction defining the angles θ_K^* and Φ, as well as the coordinate system used to define the polarization formalism.

For the case of a polarized electron beam with helicity h, the cross section form of Eq.(1) is modified to include an additional term:

$$\frac{d\sigma}{d\Omega_K^*} = \sigma_0 + h\sqrt{\epsilon(1-\epsilon)}\sigma_{LT'}\sin\Phi. \tag{3}$$

The electron beam polarization produces a fifth structure function $\sigma_{LT'}$ that is related to the beam helicity asymmetry via:

$$A_{LT'} = \frac{\frac{d\sigma^+}{d\Omega_K^*} - \frac{d\sigma^-}{d\Omega_K^*}}{\frac{d\sigma^+}{d\Omega_K^*} + \frac{d\sigma^-}{d\Omega_K^*}} = \frac{\sqrt{\epsilon(1-\epsilon)}\sigma_{LT'}\sin\Phi}{\sigma_0}, \tag{4}$$

where the $\pm$ superscripts on $\frac{d\sigma}{d\Omega_K^*}$ correspond to the electron helicity states of $h = \pm 1$.

The unpolarized cross section is determined by squares of the transverse and longitudinal amplitudes for KY electroproduction. For this reason the unpolarized cross section is Φ independent. Interferences between the KY electroproduction amplitudes of different photon helicities generate the Φ-dependent terms. The structure function σ_{TT} is determined by interference between amplitudes with transverse photons of opposite helicities. The terms σ_{LT} and $\sigma_{LT'}$ arise from the interference between the amplitudes with transverse and longitudinal photons. The polarized structure function $\sigma_{LT'}$ is intrinsically different from the structure functions of the unpolarized cross section. This term is generated by the imaginary part of terms involving the interference between longitudinal and transverse components of the hadronic and leptonic currents, in contrast to σ_{LT}, which is generated by the real part of the same interference. $\sigma_{LT'}$ is non-vanishing only if the hadronic tensor is antisymmetric, which will occur in the presence of rescattering effects, interferences between multiple resonances, interferences between resonant and non-resonant processes, or even between non-resonant processes alone [65]. $\sigma_{LT'}$ could be non-zero even when σ_{LT} is zero. When the reaction proceeds through a channel in which a single amplitude dominates, the longitudinal-transverse response will be real and $\sigma_{LT'}$ will vanish. Both σ_{LT} and $\sigma_{LT'}$ are necessary to fully unravel the longitudinal-transverse response of the K^+Y electroproduction reactions.

The bin-centered differential cross section for each hyperon final state in each kinematic bin i is computed using the form:

$$\frac{d\sigma_i}{d\Omega_K^*} = \frac{1}{\Gamma_v} \cdot \frac{1}{(\Delta Q^2 \Delta W \Delta\cos\theta_K^* \Delta\Phi)} \cdot \frac{R_i \cdot N_i \cdot BC_i}{\eta_i \cdot N_0} \cdot \frac{1}{(N_A \rho t / A_w)}, \tag{5}$$

where Γ_v is the virtual photon flux factor (using the definition from Ref. [66]) for each bin at the bin-averaged mean of the bin and is given by:

$$\Gamma_v = \frac{\alpha}{4\pi} \frac{W}{M_p^2 E^2} \frac{W^2 - M_p^2}{Q^2} \frac{1}{1-\epsilon}. \tag{6}$$

$\Delta Q^2 \Delta W \Delta\cos\theta_K^* \Delta\Phi$ is the volume of the analysis bin (with bin sizes corrected for kinematic limits in the threshold W bins), R_i is the radiative correction factor, N_i is the background-subtracted K^+Y yield in each bin, BC_i is the bin-centering factor that evolves the measured bin-averaged differential cross section over each bin to a specific kinematic point within the Q^2, W, $\cos\theta_K^*$, Φ bin, and η_i accounts for the detector geometrical acceptance and efficiency corrections. N_0 is the live-time corrected incident electron flux determined from the Faraday Cup charge summed over all data runs. Finally, $N_A \rho t / A_w$ represents the target number density, where N_A is Avogadro's number, ρ is the target density, t is the target length, and A_w is the atomic weight of the target. Further details on each of these factors is included in Ref. [44].

As for all electroproduction data, the raw cross sections will be subjected to radiative corrections in order to extract the final differential cross sections. These corrections are typically at the level of 10% to 20%. The radiative correction procedure for exclusive processes

is well established [67], and has been used in all of the analyses of the CLAS electroproduction cross sections. As has been recently demonstrated [39], radiative corrections are very important for the analysis of exclusive processes in terms of resonance excitations as they affect both the polar and azimuthal angular dependencies. This is particularly important in the extraction of the separated U, LT, and TT structure functions from the differential cross sections, which involves a Φ moment analysis (see e.g. Refs. [39, 42, 44]). Further development in radiative correction procedures based on realistic estimates of the hadronic tensors for the studies of exclusive processes is in progress [68].

Fits to the Φ dependence of the differential cross sections for the $K^+\Lambda$ and $K^+\Sigma^0$ final states will be carried out to determine the separated structure functions σ_U, σ_{TT}, and σ_{LT}. Fits to the beam spin asymmetry will be carried out to determine the polarized structure function $\sigma_{LT'}$. The separated structure functions will be extracted as a function of Q^2, W, and $\cos\theta^*_K$, using the well-established techniques that were developed from analyses of these same final states from the CLAS program [42, 44]. Note that a Rosenbluth separation is not practical in these kinematics at E_b=6.6 GeV and 8.8 GeV due to the limited ϵ lever arm. However, a separation of σ_L and σ_T is not required for this proposal as the longitudinal amplitudes are probed with greater sensitivity from the interference structure functions σ_{LT} and $\sigma_{LT'}$.

In the $K^+\Lambda$ reaction, the Λ decays weakly into a pion and a nucleon. Due to the nature of the weak decay, the decay nucleons are constrained to move preferentially in the direction of the hyperon spin. More precisely, the mesonic decay of the free Λ has an asymmetric angular distribution with respect to the spin direction of the Λ. This asymmetry is the result of an interference between parity non-conserving (s-wave) and parity-conserving (p-wave) amplitudes. In the hyperon CM frame, the decay nucleon angular distribution is therefore of the form [69]:

$$\frac{dN}{d\cos\theta_p^{RF}} = N(1 + \alpha_\Lambda P_\Lambda \cos\theta_p^{RF}), \tag{7}$$

where P_Λ is the magnitude of the Λ polarization and θ_p^{RF} is the angle between the polarization axis and the decay proton momentum in the Λ rest frame. The parameter α_Λ is the weak decay asymmetry parameter given by α_Λ=0.642 [18]. This analysis will exclusively study the dominant $p\pi^-$ decay branch (B.R.=64%) of the Λ hyperon. For the $K^+\Sigma^0$ reaction, the Σ^0 follows the decay chain $\Sigma^0 \to \gamma\Lambda$ (B.R.=100%), with $\Lambda \to N\pi$. Again, the angular distribution of the decay nucleon from the Λ follows from Eq.(7). However, α_Λ is replaced by $\alpha_\Sigma = -0.164$ (see Ref. [47] for details).

The hyperon polarization is a vector whose components can be projected onto a set of coordinate axes, referred to as the spin-quantization axes. For the formalism provided here, the primed-coordinate system of Fig. 12 has been chosen. Each of the hyperon polarization components, $P_{x'}$, $P_{y'}$, and $P_{z'}$, can be split into a beam helicity-independent part, called the *induced* polarization, and a beam helicity-dependent part, called the *transferred* polarization. This can be written as:

$$P_{i'} = P^0_{i'} + hP'_{i'}. \tag{8}$$

To accommodate finite bin sizes and to improve statistics, our analysis will be performed by summing over all relative angles Φ between the electron and hadron planes just as was

done for the analyses of Refs. [46, 47]. Using the script symbol $\mathcal{P}$ to represent the Φ-integrated Λ polarization components, they can be expressed in the (x', y', z') system in terms of the response functions as shown in Table 1 [47]. In performing the integration over Φ, the polarization components $\mathcal{P}^0_{x'}$, $\mathcal{P}^0_{z'}$, and $\mathcal{P}'_{y'}$ are equal to zero. In Table 1, the normalization term $K_I = 1/(R^{00}_T + \epsilon R^{00}_L)$.

$\mathcal{P}^0_{x'}$	0	$\mathcal{P}'_{x'}$	$K_I\sqrt{1-\epsilon^2}R^{x'0}_{TT'}$
$\mathcal{P}^0_{y'}$	$K_I(R^{y'0}_T + \epsilon R^{y'0}_L)$	$\mathcal{P}'_{y'}$	0
$\mathcal{P}^0_{z'}$	0	$\mathcal{P}'_{z'}$	$K_I\sqrt{1-\epsilon^2}R^{z'0}_{TT'}$

Table 1: Hyperon polarization components $\mathcal{P}_i$ in the (x', y', z') system integrated over Φ.

The induced polarization in a given Q^2, W, $\cos\theta^*_K$ kinematic bin for a given polarization coordinate can be extracted by forming the forward-backward yield asymmetry with respect to $\cos\theta^{RF}_p = 0$. Integrating Eq.(7) from 0 to 1 (forward) and -1 to 0 (backward) gives the corresponding yields N^F and N^B. The induced polarization can be expressed in terms of the forward-backward asymmetry A_i with respect to a given spin-quantization axis $i = x', y', z'$ using

$$\mathcal{P}^0_i = \frac{2A_i}{\alpha} = \frac{2}{\alpha}\frac{N^F - N^B}{N^F + N^B}. \tag{9}$$

For the beam-recoil transferred polarization measurement, Eq.(7) is used forming the beam helicity-gated asymmetry for a given kinematic bin with respect to a given spin quantization axis i as:

$$A_i = \frac{N^+ - N^-}{N^+ + N^-} = \alpha P_b \mathcal{P}' \cos\theta^{RF}_p, \tag{10}$$

The slope of a linear fit to the A_i vs. $\cos\theta^{RF}_p$ distribution then yields the transferred hyperon polarization components.

4.3 Stage 2 Analysis

In the second stage of the analysis, the N^* and Δ^* electrocoupling parameters will be extracted from fits to the separated structure function and polarization data using either an existing reaction model such as the Regge plus resonance model from Ghent [50] (updated to provide for a reasonable description of the data) or a phenomenological approach that is analogous to those developed in recent years for analysis of the CLAS $N\pi$ and $N\pi\pi$ datasets. These include the UIM isobar model [70] and an approach based on dispersion relations for the $N\pi$ channel [71]. For the $N\pi\pi$ channel the JM data-driven meson-baryon model has been developed [72, 73]. This approach allowed for the establishment of all essential contributing mechanisms, analyzing their manifestations in the measured observables as the peaks in the invariant mass distributions, pronounced dependencies in the angular distributions, and the correlations between the shapes of the cross sections from the different contributing mechanisms in different observables.

A critical aspect of this proposal is not just the measurement of the differential cross sections and separated structure functions for the $K^+\Lambda$ and $K^+\Sigma^0$ final states, but the development of a reaction model capable of describing the observables with sufficient accuracy to reliably extract the electrocoupling parameters for the dominant N^* and Δ^* states coupling to these channels. At the current time a reliable reaction model that accurately describes the existing CLAS $K^+\Lambda$ and $K^+\Sigma^0$ structure functions does not yet exist. This can clearly be seen from the comparisons of the available models to the data in Figs. 8 to 11.

In order to extract the N^* electrocoupling parameters from the data, it is essential that we have a flexible reaction model that can be tuned to precisely fit the existing CLAS KY photo- and electroproduction data and that eventually allows us to extract the N^* electrocouplings and their partial KY decay widths, fitting them to observables measured in the KY channels. One candidate is the Ghent Regge plus resonance (RPR) model [50] that represents a single-channel model for KY photo- and electroproduction that is based mainly on fits to the available CLAS KY photoproduction data. This hybrid approach combines a standard effective Lagrangian isobar model to describe the s-channel N^* resonance contributions with a Reggeon-exchange formalism to describe the non-resonant t-channel background. This model has been constrained by fits to the available CLAS $\gamma p \to K^+\Lambda$ and $\gamma p \to K^+\Sigma^0$ data and thus provides a good description of the photoproduction data. As of yet, the model has not been constrained by fits to any of the available CLAS electroproduction data. However, a recent effort from the Ghent group has taken important steps to use the electroproduction data to better constrain the non-resonant amplitudes above the resonance region [74]. It is expected that this development will be able to better constrain the resonant and non-resonant contributions within the resonance region.

Given the present lack of broad agreement between the RPR model and the data, there are a number of steps that will need to be undertaken to develop the RPR model (or other suitable model) into a tool that can be used to extract the N^* electrocoupling parameters for the KY final states from both the low Q^2 CLAS data and the high Q^2 CLAS12 data (including those from E12-06-108A [7]. These steps include:

1. To detail the complete list of N^* states included in the most recent version of the model along with their electrocoupling parameters for both the $K^+\Lambda$ and $K^+\Sigma^0$ final states.

2. In order to provide consistency with the electrocoupling parameters determined from fits to the CLAS $N\pi$ and $N\pi\pi$ data sets, update the model with the N^* parameters from these analyses. Depending on how different these new parameters are from what is already included in the model, new data fits may have to be performed to re-establish the model resonant/non-resonant parameters.

3. In order to develop a true extraction model from the available reaction model, refit the model to the CLAS photo- and electroproduction data (Q^2 up to 4 GeV^2) with the existing non-resonant parameters constrained to their measured uncertainties and extract the electrocoupling parameters and KY decay widths for all prominent N^* states that couple to the $K^+\Lambda$ and $K^+\Sigma^0$ exclusive channels. Given the significant amount of data involved, this work will require studies of the stability of the fit results and the sensitivities to the different data sets given their quoted systematic uncertainties.

This work will eventually lead to a fourth goal to further develop the model to be able to include the new KY data for W up to 3 GeV and Q^2 up to 10 - 12 GeV^2 that can be used as input for coupled-channel model development in these kinematics. Work to develop this reaction model is now getting underway and the plan is to have it sufficiently developed on a time-scale appropriate for the new measurements from this proposal. The development of the RPR model along this direction was presented in Ref. [75].

The extraction of the electrocoupling amplitudes for those N^* states that couple to the KY channels will be completed separately for both the $K^+\Lambda$ and $K^+\Sigma^0$ channels as a function of Q^2. These results can be compared with the $\gamma_v NN^*$ electrocouplings available from the studies of the $N\pi\pi$ channel. These fits will provide a set of initial N^* electrocoupling amplitudes. A final evaluation of N^* electrocoupling amplitudes will be carried out within the framework of the most advanced coupled-channel approaches, which are currently being developed by the Argonne-Osaka Collaboration [4] and the GWU group [76] (members of which are part of the group supporting this proposal). Both of these approaches account for the contributions of all relevant meson-baryon open channels and their hadronic interactions. Ultimately, they will include updates from JPARC data on the (π, K) and (K, π) reaction channels at W values covered by this proposal [77]. Consistent results on the $\gamma_v NN^*$ electrocouplings from independent analyses of the $N\pi$, $N\pi\pi$ and KY channels and extracted from the global coupled-channel analysis will provide the final reliable extraction of these fundamental quantities. We also expect significant contributions from the JPAC group at JLab [33] that will help to develop analysis methods for interpreting the extracted N^* form factors for Q^2 up to 12 GeV^2 in terms of DSE and LQCD predictions.

4.3.1 Legendre Analysis

In order to investigate in a cursory manner the evidence for N^* resonance couplings in the separated structure functions for the CLAS data at $Q^2 < 4$ GeV^2, a series of Legendre polynomial fits were carried out [44]. The first approach fit the individual structure functions σ_U, σ_{LT}, σ_{TT}, and $\sigma_{LT'}$ versus $\cos\theta_K^*$ for each Q^2 and W point for the $K^+\Lambda$ and $K^+\Sigma^0$ final states using a truncated series of Legendre polynomials as:

$$C_{\ell=0\rightarrow 3} = \int_{-1}^{+1} \frac{d\sigma_{U,LT,TT,LT'}}{d\Omega^*} P_\ell(\cos\theta_K^*)\ d\cos\theta_K^*. \tag{11}$$

The fit coefficients for $\ell = 0 \rightarrow 3$ are shown for $K^+\Lambda$ in Fig. 13 and for $K^+\Sigma^0$ in Fig. 14 for $Q^2 = 1.80$ GeV^2. It is expected that the appearance of a structure in a single C_ℓ coefficient at the same W value and in each of the Q^2 points is likely a signal of an N^* contribution. Note that the appearance of a structure at a given value of W for each of the different C_ℓ coefficients most likely suggests the presence of a dynamical effect rather than the signature of an N^* contribution.

The fits for $K^+\Lambda$ show structures for each of the three Q^2 points in the analysis ($Q^2 = 1.80$, 2.60, 3.45 GeV^2) at W=1.7 GeV in C_0 for both σ_U and σ_{LT}, W=1.9 GeV in C_2 and C_3 for σ_U, and W=2.2 GeV in C_3 for σ_U. The fits for $K^+\Sigma^0$ show structures at W=1.9 GeV in C_0 and C_2 for σ_U and σ_{TT}. Note that in the Bonn-Gatchina partial wave analysis, these two structures have been identified as coming from the $N(1710)\frac{1}{2}^+$ and a new $N(1900)\frac{3}{2}^+$ state based on fits including the CLAS $K^+\Lambda$ photoproduction data. In the amplitude fit of the CLAS $K^+\Lambda$ photoproduction data [78], a resonant structure in the D-wave at 2.2 GeV has been

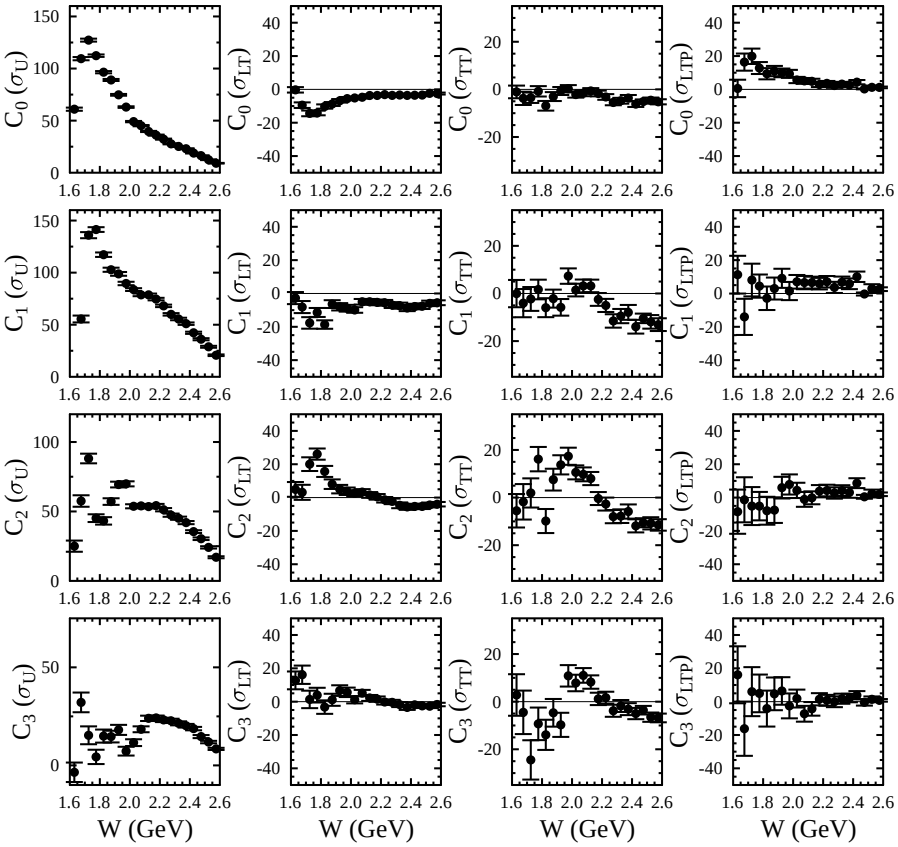

Figure 13: Legendre polynomial fit coefficients (nb) for $\ell = 0 \rightarrow 3$ vs. W for the $K^+\Lambda$ separated structure functions σ_U, σ_{LT}, σ_{TT}, and $\sigma_{LT'}$ for Q^2=1.80 GeV^2 [44].

identified. Of course, making statements regarding the possible orbital angular momentum of the associated resonances requires care as interference effects among the different partial waves can cause strength for a given orbital angular momentum value to be spread over multiple Legendre coefficients. For the $K^+\Sigma^0$ fits, strength is seen at W=1.85 GeV in C_0 and W=1.9 GeV in C_2. It is interesting that there is no signature of strength in the P-wave as seen through the coefficient C_1, but again a more sophisticated and complete analysis will be required to make more definitive statements. Regardless of the details and issues, these studies indicate the sensitivity of the KY final states to high-lying N^* couplings.

4.4 Monte Carlo Simulation Studies

In order to study the detector response and to model the CLAS12 acceptance function for this proposal, the standard CLAS12 fast Monte Carlo (fastMC) suite was employed. This simulation code included the nominal detector geometries and the expected position and time resolutions for the detectors for the reconstruction of the four-momenta of the final state particles. The event generator was based on the PYTHIA6 phase space model [79] modified to reflect the expected Q^2 dependence of the incident virtual photon flux and the t-dependence ($t = (p_{\gamma^*} - p_K)^2$) of the final state K^+ seen from Ref. [44]. Fig. 15 shows the kinematics of the reconstructed Monte Carlo events at a beam energy E_b=6.6 GeV as a function of Q^2, W, and $\cos\theta^*_K$. The corresponding distributions of these quantities

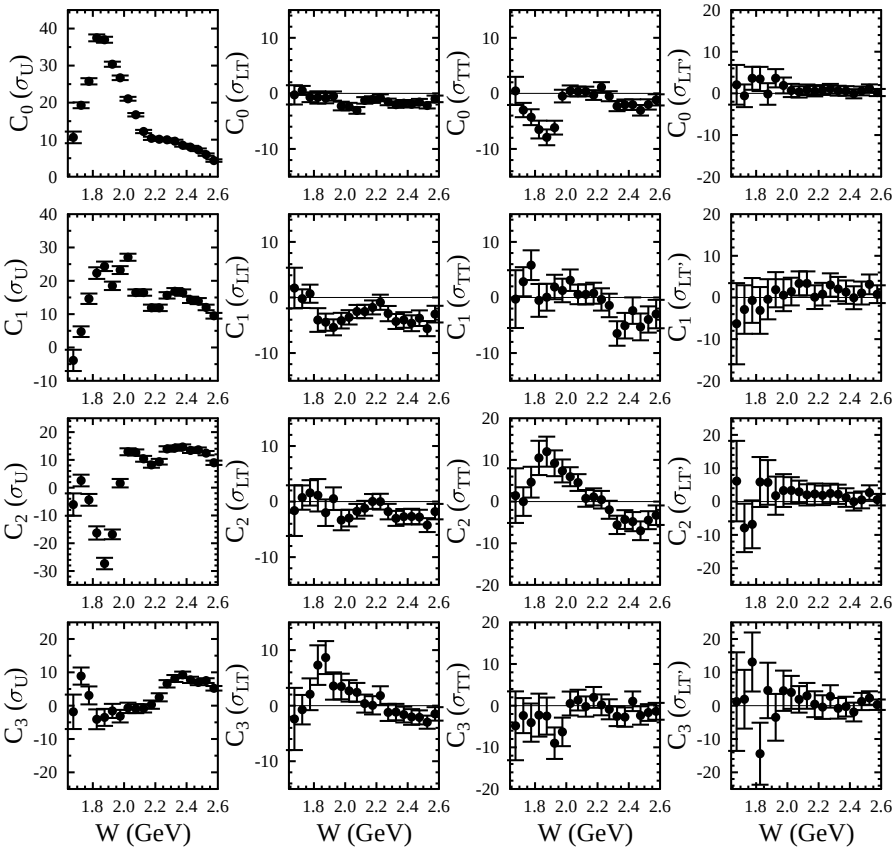

Figure 14: Legendre polynomial fit coefficients (nb) for $\ell = 0 \rightarrow 3$ vs. W for the $K^+\Sigma^0$ separated structure functions σ_U, σ_{LT}, σ_{TT}, and $\sigma_{LT'}$ for Q^2=1.80 GeV^2 [44].

reconstructed from the CLAS e1f dataset at E_b=5.5 GeV are shown in Fig. 16 for comparison. Fig. 15 shows that the Q^2 and W distributions match the reaction phase space as compared to the CLAS e1f data from Fig. 16. The differences are due to different beam energies (6.6 GeV vs. 5.5 GeV) and due to the use of the phase-space event generator. The $\cos\theta^*_K$ distribution from Monte Carlo shows the strong forward-peaking as the CLAS data but has two notable features. The first is a different behavior as $\cos\theta^*_K \rightarrow 1$ due to the different torus polarities (the CLAS12 simulations used a negative torus polarity and the CLAS data was taken with a positive torus polarity). The second is a dip at $\cos\theta^*_K \approx -0.2$ due to the acceptance gap between the CLAS12 forward and central detectors that is exacerbated by the negative torus polarity. The p vs. θ laboratory distributions for the final state charged particles e', K^+, p, and π^- are shown in Fig. 17. The e', K^+, and p are mostly directed toward the CLAS12 forward detector system ($\theta < 35^\circ$), while the accepted π^- tracks are mostly contained within the CLAS12 central detector system ($\theta > 35^\circ$).

Figure 18 shows the particle identification capabilities expected for the CLAS12 Forward Time-of-Flight (FTOF) system based on the flight time differences between charged hadrons as a function of momentum. The primary issue with the final state reconstruction will be separating K^+ tracks from the dominant π^+ background. The FTOF system was designed to separate K^+ tracks from π^+ tracks up to $\sim$3 GeV with 4σ separation (assuming an average FTOF resolution of 80 ps). However, 1σ separation based on the nominal system design up to 6 GeV is provided. However, these statements are believed to be conservative. Based

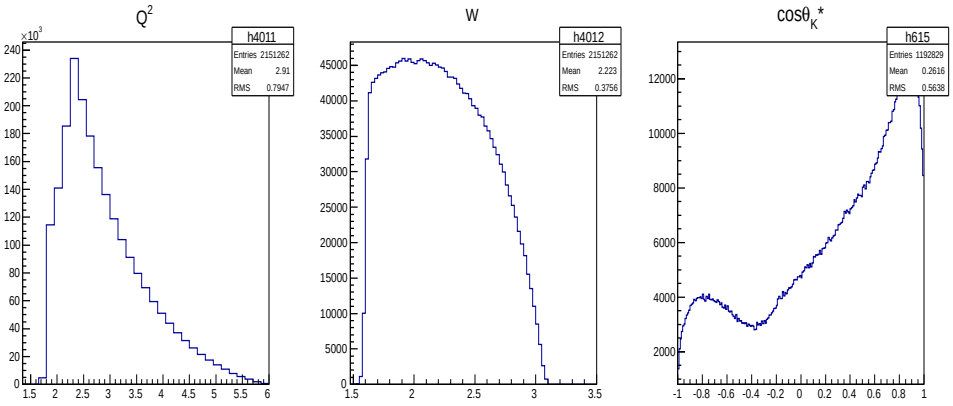

Figure 15: Yield distributions of Q^2, W, and $\cos\theta^*_K$ for the reconstructed Monte Carlo events from the modified K^+Y phase space generator at E_b=6.6 GeV with the torus set at $B = 0.9B_{max}$ for negatively charged particles outbending used to determine the CLAS12 acceptance functions for this proposal. Note that the sharp edges seen in the Q^2 and W distributions here are due to the kinematic bounds selected for the event generation.

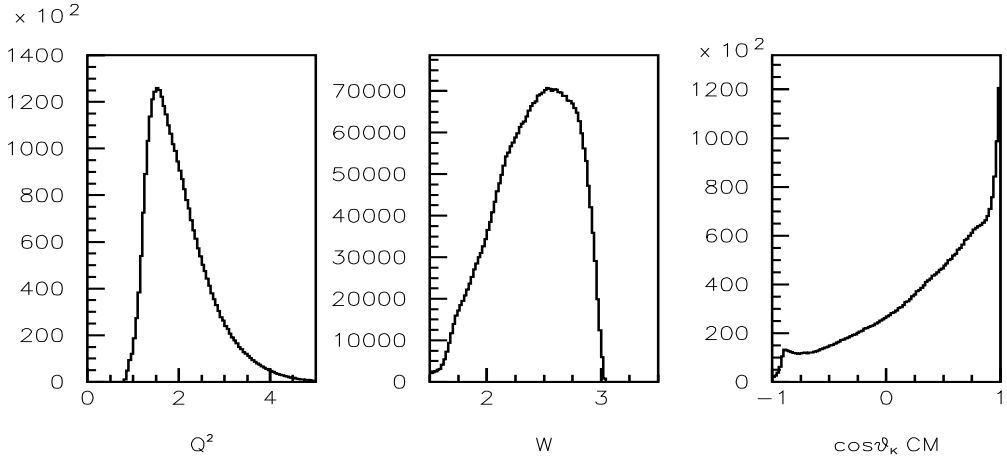

Figure 16: Yield distributions of Q^2, W, and $\cos\theta^*_K$ for the CLAS e1f dataset at E_b=5.5 GeV for K^+Y events with the torus set at $B = 0.9B_{max}$ with negatively charged particles inbending.

on the measured resolutions for the new FTOF panel-1b counters, 2σ separation of π/K tracks up to 6 GeV should be achievable. The average timing resolution of the new FTOF panel-1b system is ∼50 ps (δt=30 ps at small angles to 80 ps at large angles). The timing resolution of the FTOF system is expected to improve by an additional ∼20% when the timing information from the panel-1b arrays is combined with that for the panel-1a arrays located immediately downstream of panel-1b. Details on the FTOF system performance are available in Ref. [80]. Final state K^+ identification will thus rely heavily on the FTOF particle identification capabilities over the full K^+ momentum range.

Particle identification in CLAS12 in the forward direction is actually accomplished through the use of multiple detection subsystems, including not only the FTOF, but also the two Cherenkov detector systems, the Low Threshold Cherenkov Counter (LTCC) and the High Threshold Cherenkov Counter (HTCC), and in one sector a Ring Imaging Cherenkov Detector (RICH). Fig. 19 shows a representation of which subsystems are nominally employed for

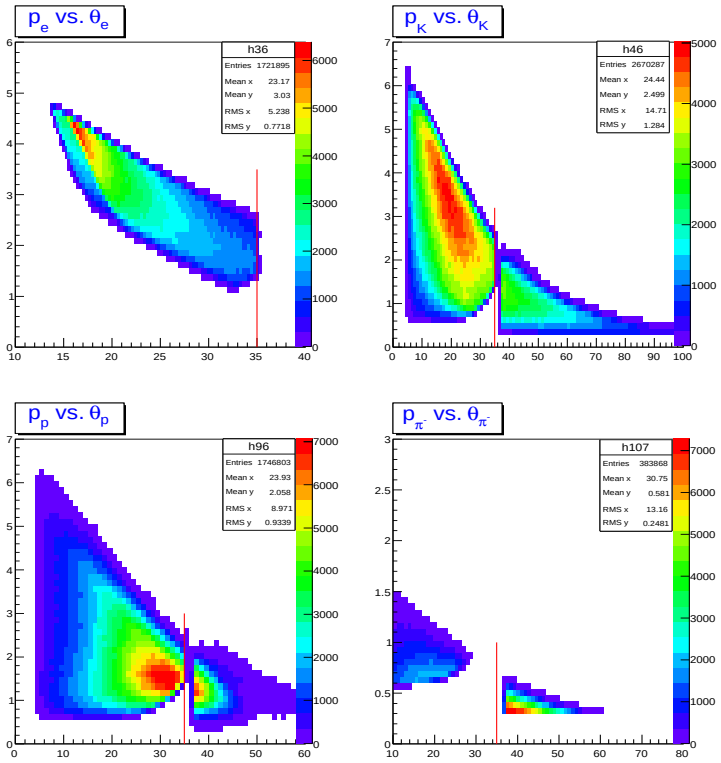

Figure 17: Yield distributions of laboratory momentum (GeV) vs. polar angle (deg) from reconstructed Monte Carlo data for the final state e' (UL), K^+ (UR), p (LL), and π^- (LR) for the reaction $ep \rightarrow e'K^+\Lambda$ at E_b=6.6 GeV with the torus set at $B = 0.9B_{max}$ for negatively charged particles outbending. The discontinuity at $\theta = 35^\circ$ (noted by the vertical red lines) is due to the acceptance gap between the CLAS12 forward and central detectors.

charged hadron identification as a function of momentum. The LTCC in its nominal active area is expected to be 95% - 99% efficient for π/K separation in the range of momenta from 3 GeV to 9 GeV. The HTCC is expected to be 95% - 99% efficiency for π tracks from 5 GeV to 9 GeV. The RICH is designed to be highly efficient to separate pions from kaons from 3 GeV to 8 GeV. Note that the RICH will be employed if it is available, but it is not a required element of this proposal.

The momentum distribution for the final state K^+ is important to consider given the particle identification capabilities of CLAS12. The reconstructed K^+ momenta will be in the range from 0.5 GeV to 7 GeV. Fig. 20 shows the K^+ momenta as a function of Q^2 from our Monte Carlo data over the kinematic range of this proposal. The average K^+ momentum is $\sim 2-4$ GeV, with a relatively weak dependence on Q^2.

The nominal analysis scheme will identify the exclusive reaction channel by detection of the final state e' and K^+. However, the detection of the final state proton from the Λ hyperon mesonic decay (B.R.=64%) will allow us to further reduce the underlying backgrounds employing a cut on the $MM^2(e'K^+p)$ distribution to select events with a missing π^- or a missing $\pi^-\gamma$ (see Fig. 21). This will allow for fits that separate the $K^+\Lambda$, $K^+\Sigma^0$, and background contributions with different systematics. Comparison of cross sections extracted using the $e'K^+$ final state topology to that from the $e'K^+p$ final state topology will be used to assess the systematic uncertainties associated with the background subtraction and fitting

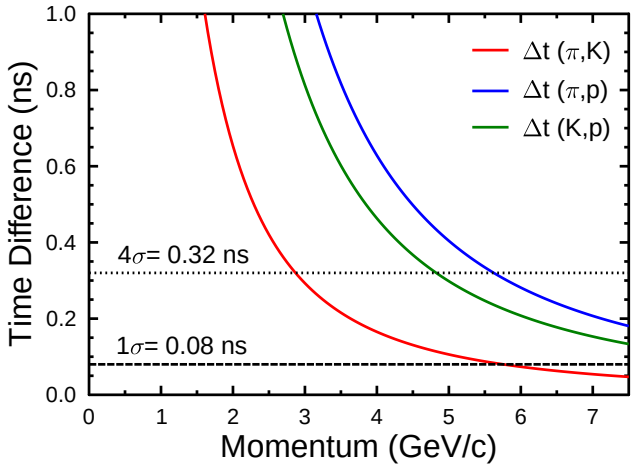

Figure 18: Difference in charged hadron flight times from the event vertex to the FTOF system as a function of hadron momentum showing the differences between π/K (red curve), π/p (blue curve), and K/p (green curve). The 4σ and 1σ FTOF time resolution lines are shown.

algorithms used to separate the $K^+\Lambda$ and $K^+\Sigma^0$ event samples from the $e'K^+$ missing mass distributions for each bin of Q^2, W, $\cos\theta^*_K$, and Φ.

For this proposal the fastMC studies have shown that the CLAS12 acceptance for both $e'K^+$ and $e'K^+p$ final states is fairly flat for torus field settings from $B = 0.4B_{max}$ to $B = 0.9B_{max}$. The acceptance for positive polarity torus operation (negatively charged particles bending inward) is seen to be ~10% higher than for reversed field running. However, the reversed torus polarity configuration has been assumed in the Monte Carlo studies as this is the configuration that has been chosen for this run group. However, while the acceptance dependence on the torus configuration is relatively small, the biggest affect on the KY analysis versus torus field strength is the missing mass resolution function. The average CLAS12 missing mass resolution at $0.4B_{max}$ is 30 MeV, at $0.6B_{max}$ is 22 MeV, and at $0.9B_{max}$ is 15 MeV. Representative hyperon missing mass spectra for the detected $e'K^+p$ final state topology are shown in Fig. 22. For these studies, three different reactions were simulated, including the hyperon channels of interest, $K^+\Lambda$ and $K^+\Sigma^0$, as well as the predominant background channel $ep \rightarrow e'p\pi^+\pi^-$, where the final state π^+ is misidentified as a K^+. The non-leading impact of the accidental background is discussed in detail in Section 4.5. These studies employed $N_{K\Lambda}/N_{K\Sigma}$=2 based on the ratios seen in the CLAS e1c and e1f datasets (which span 0.5 GeV^2 < Q^2 < 3.9 GeV^2, W up to 2.6 GeV). The background channel was assumed to have three times the integrated yield as the $K^+\Lambda$ channel in the mass range shown, again based on the findings from the CLAS e1c and e1f datasets scaled by the expected particle misidentification background expected for CLAS12 operation at $\mathcal{L} = 1 \times 10^{35}$ cm^{-2}s^{-1} (see Section 4.5).

Figure 23 shows the expected missing mass resolution of CLAS12 as a function of Q^2 and W summed over all other kinematic variables at E_b=6.6 GeV for the 3 torus field strengths of 40%, 60%, and 90% B_{max}. The resolution is relatively flat with W. However, the resolution function has a strong dependence on Q^2. Further work will be needed to develop approaches for fitting the missing mass spectra to separate the $K^+\Lambda$, $K^+\Sigma^0$, and background channels.

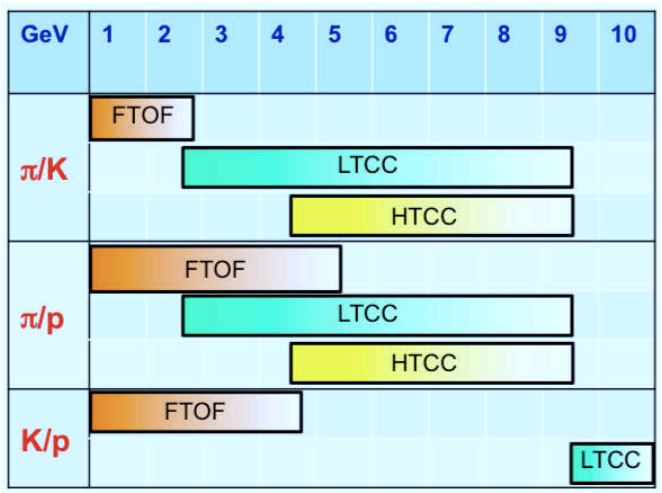

Figure 19: Representation of which CLAS12 subsystems are employed for charged hadron identification as a function of momentum. Note that for one sector on the CLAS12 Forward Carriage the LTCC will be replaced by a RICH detector.

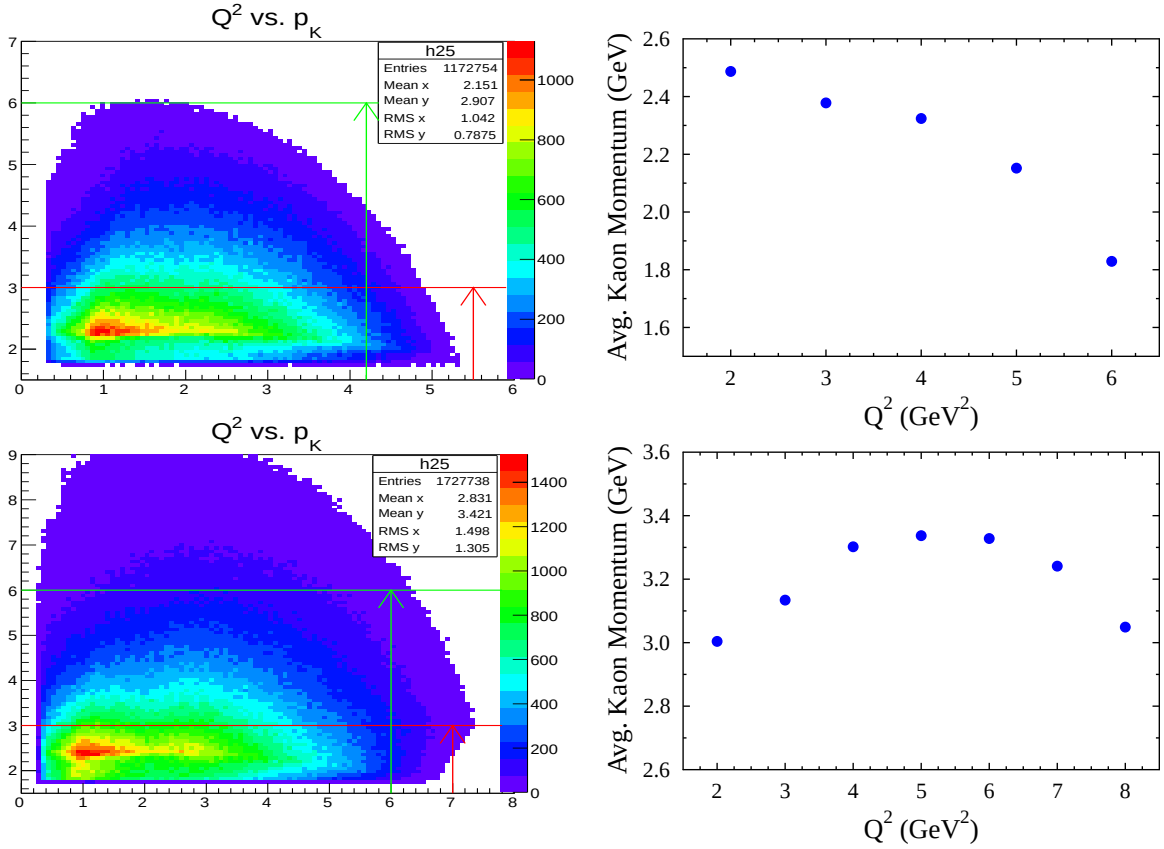

Figure 20: Yield distributions of Q^2 vs. K^+ momentum (left) and the average K^+ momentum vs. Q^2 (right) for E_b=6.6 GeV (top) and E_b=8.8 GeV (bottom) with the torus set at $B = 0.9B_{max}$ for negatively charged particles outbending for K^+Y events from reconstructed Monte Carlo data. The CLAS12 particle identification capabilities based on timing measurements alone provide for 4σ π/K separation up to the red horizontal line and for 1σ π/K separation up to the green horizontal line.

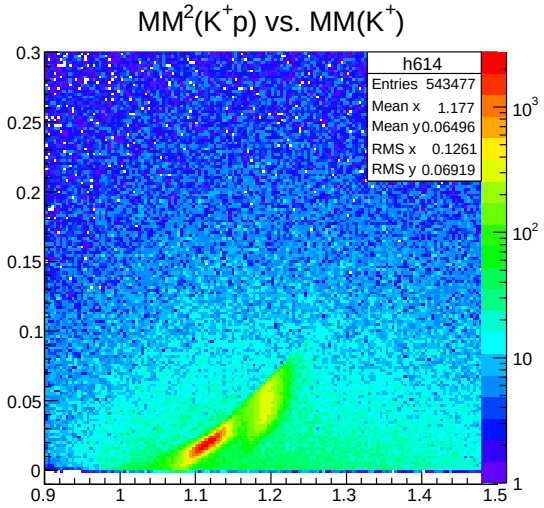

Figure 21: Correlation of the reconstructed $MM^2(e'K^+p)$ (GeV^2) vs. $MM(e'K^+)$ (GeV) distributions at E_b=6.6 GeV from reconstructed Monte Carlo with the torus set at $B = 0.9B_{max}$ for negatively charged particles outbending.

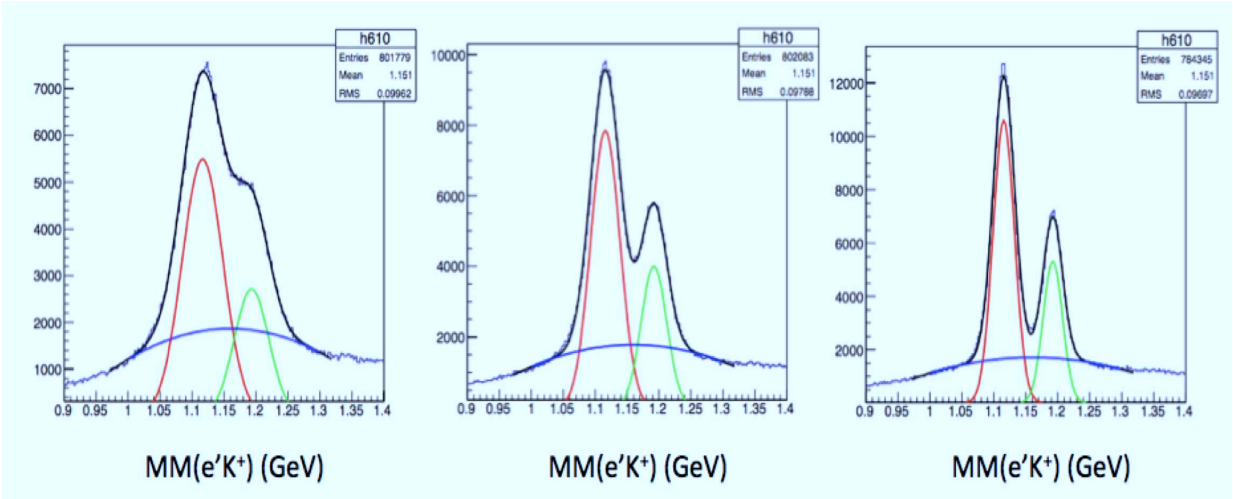

Figure 22: Missing mass spectra $MM(e'K^+)$ for the reconstructed $e'K^+p$ final state topology for reversed torus magnet polarity with $B = 0.4B_{max}$ (left), $B = 0.60B_{max}$ (middle), and $B = 0.9B_{max}$ (right) for the expected ratios of $K^+\Lambda$, $K^+\Sigma^0$, and background events. The histograms are overlaid with lineshape fits.

However, the algorithms successfully employed for the analysis of Ref. [44] will be used as a starting point. Note as well that the fastMC does not account for radiative effects that will increase the degree of overlap of the hyperon peaks in the $MM(e'K^+)$ spectrum. However, in these kinematics the radiative effects are not expected to significantly affect the spectrum as reflected in Fig. 22. This statement is also consistent with our previous experience on the impact of radiative effects under similar conditions [44].

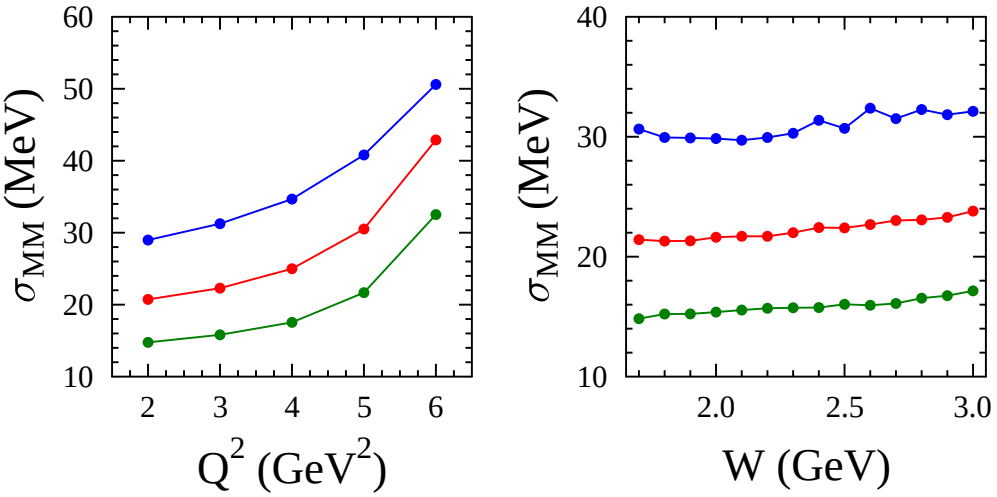

Figure 23: Hyperon missing mass $MM(e'K^+)$ resolution from reconstructed $ep \rightarrow e'K^+\Lambda$ Monte Carlo data as a function of (left) Q^2 (averaged over W and $\cos\theta^*_K$) and (right) W (averaged over Q^2 and $\cos\theta^*_K$). The blue curves are for $B = 0.4B_{max}$, the red curves are for $B = 0.60B_{max}$, and the green curves are for $B = 0.9B_{max}$.

Separation of the $K^+\Lambda$ and $K^+\Sigma^0$ event samples will proceed using a fitting approach that accounts for the CLAS12 resolution function as a function of Q^2 and W as alluded to above. With detection of only the final state $e'K^+$ or $e'K^+p$, kinematic fitting does not have sufficient constraints to enable a complete event-by-event separation of the $K^+\Lambda$, $K^+\Sigma^0$, and background channels. In fact, kinematic fitting is not expected to lead to any significant improvement relative to a careful spectrum fitting approach. However, investigations of kinematic fitting approaches and studies of their effectiveness for CLAS12 and for these specific final states will be further considered.

4.5 Event Backgrounds

The backgrounds within the $e'K^+$ missing mass distributions need careful consideration in the planning of this experiment. If the CLAS12 K^+ particle identification in the event reconstruction was certain (i.e. C.L.=100%), then the contributing backgrounds would be easily be eliminated. However, there will always be a finite probability of making the wrong particle assignment in the final state reconstruction. Using a particle identification scheme based solely on timing information from the FTOF detectors, there are two possible avenues to misidentify a K^+ and a π^+:

1. The finite time resolution of the FTOF system cannot distinguish π^+ and K^+ tracks

when their flight time difference for a given momentum is on the order of the system timing resolution (see Fig. 18).

2. π^+ tracks from earlier or later beam buckets when associated with the beam bucket of the triggering electron can appear to be K^+ tracks.

For particle misidentification of the first sort, the better the system timing resolution, the smaller this contribution will be. However, for events of the second sort, the misidentification probability is not dependent on the system timing resolution.

The K^+ misidentification background will reside in the $e'K^+$ missing mass distribution and an important component will arise from accidental coincidences between scattered electrons and unrelated hadrons. These unrelated hadrons are primarily pions from neighboring beam bunches. Of course, the other important contribution will be from physics backgrounds, the dominant reaction process being $ep \rightarrow e'\pi^+\pi^- p$, where the π^+ is misidentified as a K^+. Fig. 24 shows the reconstructed $MM(e'K^+)$ distributions from CLAS data at E_b=5.5 GeV for the two final state topologies of interest, $e'K^+$ and $e'K^+p$. Note that the backgrounds beneath the hyperon peaks are significantly reduced with the inclusion of the detection of the proton.

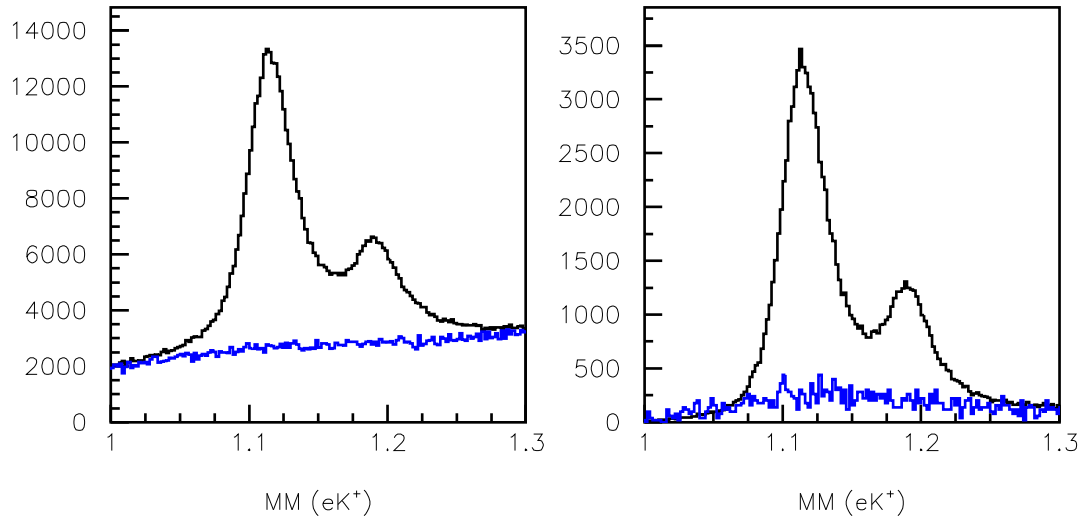

Figure 24: Hyperon missing mass $MM(e'K^+)$ distributions from CLAS e1f data at 5.5 GeV summed over all Q^2, W, and $\cos\theta^*_K$ for the $e'K^+$ topology (left) and the $e'K^+p$ topology (right) with a cut on the $MM^2(e'K^+p)$ distribution on the missing $\pi^-/\pi^-\gamma$, showing the significant reduction in particle misidentification background beneath the hyperons when additional exclusivity cuts are applied to the data. The blue histogram is the particle misidentification background contribution from the reaction $ep \rightarrow e'p\pi^+\pi^-$.

As the operating luminosity of CLAS12 will be ten times higher than for CLAS, the expected background levels might be expected to be ~10 times larger (since the accidental rate scales as the luminosity squared, which is compensated for by the ten times higher event rate that scales with the beam current). However, the issue of accidentals from misidentified K^+ is mitigated as the particle misidentification levels are reduced. In fact, the particle identification capabilities of CLAS12 are significantly improved compared to those of CLAS as:

- The timing resolution of the CLAS12 FTOF system is about a factor of three better than for the CLAS TOF system [80].

- The HTCC, LTCC, and RICH systems of CLAS12 are an important component of the hadron identification system that together are 95% $\rightarrow$ 99% efficient for π/K separation for momenta $p > 3$ GeV.

In addition, the backgrounds from particle misidentification in the $MM(e'K^+)$ spectrum are further improved during reconstruction of the final state as:

- The detection of the p from the hyperon decay with a cut on the $MM^2(e'K^+p)$ distribution on the missing π^- (for the $K^+\Lambda$ final state) and the missing $\pi^-\gamma$ (from the $K^+\Sigma^0$ final state) reduces the particle misidentification background by a factor of $\sim$10 as shown in Fig. 24.

- The tracking vertex resolution of CLAS12 in the forward direction ($\theta < 35^\circ$) employing the drift chambers and the micro-megas is roughly a factor of five better than that using the drift chambers of CLAS (2 mm vs. 1 cm). This allows for improved resolution on the detached vertices for the $\Lambda \rightarrow p\pi^-$ decay ($c\tau = 7.89$ cm). This resolution can be expected to allow for cuts to reduce the non-strange background considerably. The development and optimization of this algorithm is planned for later this year.

Further information on accidental rates can be gleaned from our experience with operation of the CLAS detector at a luminosity of $\mathcal{L} = 1\times10^{34}$ cm^{-2}s^{-1}. The total hadronic rate in CLAS was measured to be roughly 1 MHz. For a trigger coincidence time window of 100 ns, this gives an accidental rate of 0.1 Hz. For CLAS12 operation at $\mathcal{L} = 1 \times 10^{35}$ cm^{-2}s^{-1} the accidental rate should be at the level of tens of Hz as the total hadronic rate is expected to be 5 MHz. Even in this worst case scenario, this rate is not expected to be a limiting factor for exclusive K^+Y final state reconstruction in CLAS12 as it is comparable to the KY production rates in the expected running conditions. However, the contribution of the accidental events to the $MM(e'K^+)$ spectra will be significantly less than this due to the CLAS12 hadron identification system and the cuts included to fully identify the exclusive final state. It is clear that accidental coincidences in CLAS12 for this final state will be a much smaller contribution to our $MM(e'K^+)$ spectra compared to particle misidentification events arising within the primary beam bucket that triggers the event, and the contribution of these events to the $MM(e'K^+)$ spectra in both the $e'K^+$ and $e'K^+p$ topologies are reasonably well understood based on existing CLAS data.

Our nominal approach for the analysis will be to attempt to measure the differential cross sections and separated structure functions from this experiment for the $K^+\Lambda$ and $K^+\Sigma^0$ channels in the topology where only the final state e' and K^+ are detected. This topology results in the highest acceptance for the reactions of interest. All analysis results will be cross-checked from the cross sections measurements determined from the topology that requires detection of the e', K^+, and p in the final state. This final state is, of course, necessary for the analysis to measure the induced and recoil hyperon polarizations. The $MM(e'K^+)$ spectra that could be expected from this experiment are shown requiring the $e'K^+p$ topology in Section 4.4. Although the background levels have been increased by a factor of 10 relative to what has been seen in analysis of data from CLAS (see Fig. 24), this

is believed to be a considerable over-estimate of the background levels given that we have not attempted to account for the expected reductions discussed in this section.

Further studies of particle misidentification effects will be studied employing our full CLAS12 GEANT-4 Monte Carlo suite (gemc [81]) later this year after the Monte Carlo and the CLAS12 reconstruction software package [82] are further developed.

4.6 Count Rate Estimates

The K^+Y differential cross section in a given bin of Q^2, W, $\cos\theta^*_K$, and Φ can be written as:

$$\frac{d\sigma}{d\Omega^*_K} = \frac{1}{\mathcal{L}} \cdot \frac{N}{ACC \cdot (\Delta Q^2 \Delta W \Delta \cos\theta^*_K \Delta\Phi)} \cdot \frac{1}{\Gamma_v} \cdot \frac{1}{t_R}, \tag{12}$$

where $\mathcal{L}$ is the beam-target luminosity, N is the number of counts in the bin, ACC is the CLAS12 acceptance for the bin (including all inefficiencies, branching ratios, and dead times), Γ_v is the virtual photon flux factor, and t_R is the run duration.

	E_b=6.6 GeV		E_b=8.8 GeV	
Bin	Q^2 (GeV^2)	W (GeV)	Q^2 (GeV^2)	W (GeV)
1	2.0	1.725	4.0	1.725
2	2.0	1.925	4.0	1.925
3	3.0	1.725	5.0	1.725
4	3.0	1.925	5.0	1.925
5	4.0	1.725	6.0	1.725
6	4.0	1.925	6.0	1.925
7	5.0	1.725	7.0	1.725
8	5.0	1.925	7.0	1.925

Table 2: The eight representative bins in Q^2 and W used for the count rate estimates in this proposal for the 6.6 and 8.8 GeV beam energies.

To determine the expected yields for this experiment, estimates for the $K^+\Lambda$ and $K^+\Sigma^0$ final states were carried out for the eight representative Q^2/W bins for each beam energy as shown in Table 2. These include two values of W (1.725 GeV, 1.925 GeV) and four values of Q^2, 2.0 GeV^2, 3.0 GeV^2, 4.0 GeV^2, 5.0 GeV^2 for E_b=6.6 GeV and 4.0 GeV^2, 5.0 GeV^2, 6.0 GeV^2, 7.0 GeV^2 for E_b=8.8 GeV. In addition, the following assumptions were made:

- $\mathcal{L} = 1 \times 10^{35}$ cm^{-2}s^{-1} - nominal CLAS12 design operating luminosity
- Full torus field ($B = 0.9B_{max}$) with negatively charged particles outbending
- Solenoid at full nominal field
- t_R = 50 days for E_b=6.6 GeV and 50 days for E_b=8.8 GeV
- Γ_v from Eq.(6)

- $d\sigma/d\Omega$ from a $1/Q^2$ extrapolation of the form:

$$d\sigma/d\Omega = \mathcal{C}_1 \cdot \left(\mathcal{C}_2 + Q^2\right)^{-1} \tag{13}$$

  to the electroproduction cross sections in each $\cos\theta^*_K$ bin from Ref. [44].

- Binning:
  - $\Delta Q^2 = 1.0$ GeV^2
  - $\Delta W = 50$ MeV,
  - $\Delta \cos\theta^*_K$ 10 bins:

    [-0.90,-0.65], [-0.65,-0.40], [-0.40,-0.20], [-0.20,0.00], [0.00,0.20], [0.20,0.40], [0.40,0.60], [0.60,0.75], [0.75,0.90], [0.90,1.00]
  - $\Delta\Phi$: 8 bins 45°-wide [-180°,180°]

    ($\cos\theta^*_K$ and Φ binning chosen to match e1f analysis)

- *ACC* from fastMC with a reasonably realistic event distribution for the event generator (see Section 4.4.

The acceptances in each kinematic bin were determined from the ratio of reconstructed to generated events in each bin. The acceptances determined for the $K^+\Lambda$ final state for the $e'K^+$ and $e'K^+p$ topologies are shown in Fig. 25 and Fig. 26, respectively, for the eight bins of Table 2 averaged over Φ. The acceptances for the $K^+\Sigma^0$ final state are comparable. The studies show typical Φ-averaged $e'K^+$ topology acceptances of 50% and typical Φ-averaged $e'K^+p$ topology acceptances of 25%, relatively independent of kinematics.

Figures 27 and 28 show the expected yields determined using Eq.(12) for the $K^+\Lambda$ final state for both the $e'K^+$ and $e'K^+p$ topologies for E_b=6.6 GeV and 8.8 GeV, respectively. Figs. 29 and 30 show the corresponding yields expected for the $K^+\Sigma^0$ final state. Note that for the $e'K^+p$ topology the $\Lambda \to p\pi^-$ branching ratio of 64% has been taken into account. Also shown in these figures are the measured yields from the e1f analysis at Q^2=1.8 GeV^2 (from Ref. [44]) for the $e'K^+$ topology, which we might consider as a reasonable measure of the required statistics for a viable experiment. A comparison of the expected yields from this proposed experiment at E_b=6.6 GeV and 8.8 GeV and the existing CLAS data from Ref. [44] shows an increase of a factor of 10 to 100 for the $e'K^+$ topology in the range from Q^2=2 GeV^2 to 4 GeV^2. For Q^2 in the range from 4 GeV^2 to 7 GeV^2, the expected statistics, even in the $e'K^+p$ topology, are comparable to the statistics from our already published CLAS data at Q^2=1.8 GeV^2 in the $e'K^+$ topology. These statistics are judged to be sufficient to successfully complete both the Stage 1 and Stage 2 analysis programs as described in Sections 4.2 and 4.3, respectively.

Note the $1/Q^2$ extrapolation of Eq.(13) was found to be the most reasonable to fit the existing CLAS data in the range of Q^2 up to 4 GeV^2. However, the expected yields were also studied using a $1/Q^4$ extrapolation of the cross sections in Ref. [44] as:

$$d\sigma/d\Omega = \mathcal{C}_1 \cdot \left(\mathcal{C}_2 + Q^2\right)^{-2}, \tag{14}$$

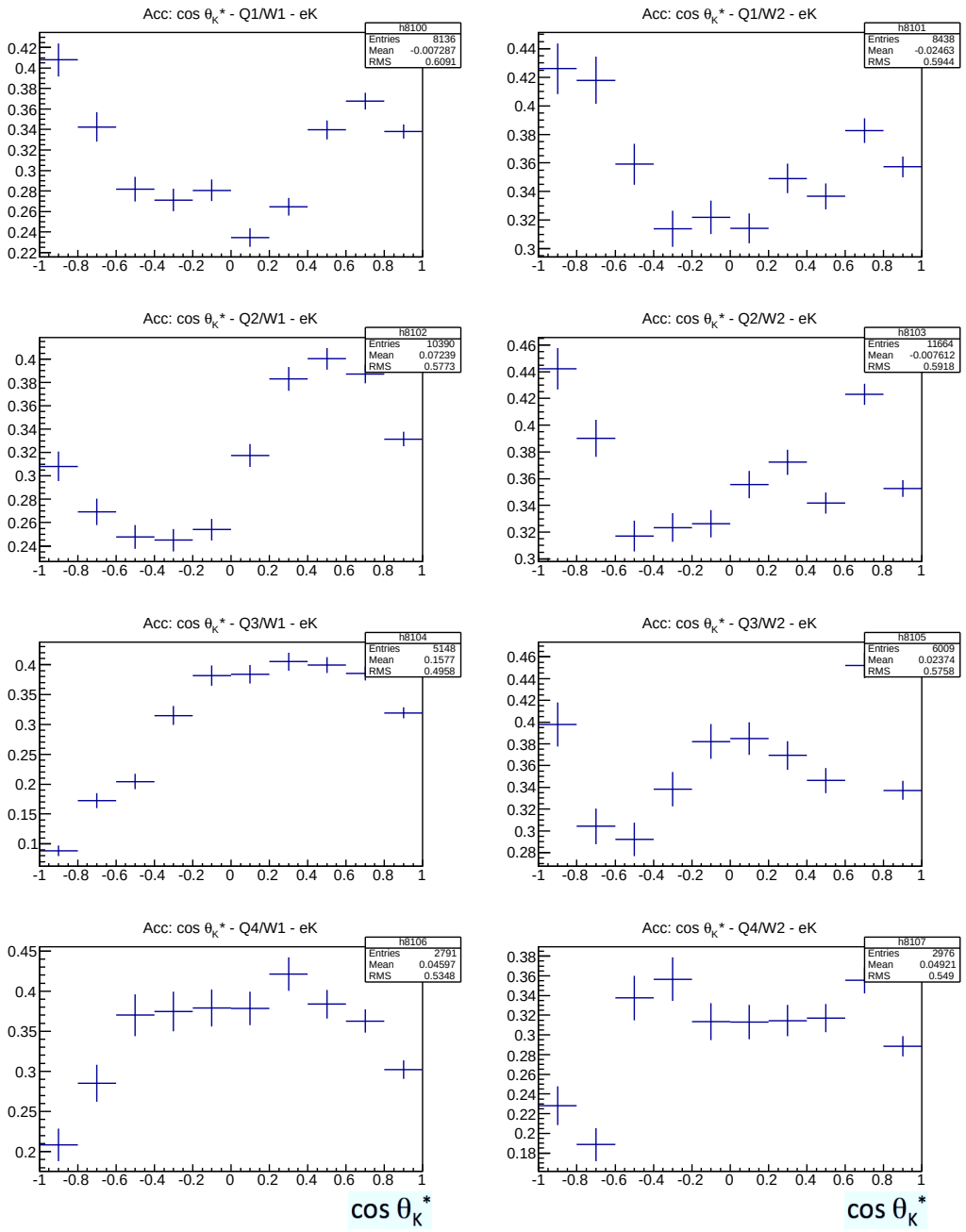

Figure 25: Acceptance functions determined from the Monte Carlo simulations for E_b=6.6 GeV with the torus set at $B = 0.9B_{max}$ for negatively charged particles outbending as a function of $\cos\theta^*_K$ averaged over Φ for the $K^+\Lambda$ final state for the $e'K^+$ topology for W=1.725 GeV (left) and W=1.925 GeV (right) for each of the four Q^2 bins listed in Table 2, Q^2=2.0 GeV^2 (top row), 3.0 GeV^2 (second row), 4.0 GeV^2 (third row), and 5.0 GeV^2 (bottom row). These acceptances were determined with a thrown event sample of 10M events and yield statistical uncertainties on the acceptance of a few percent.

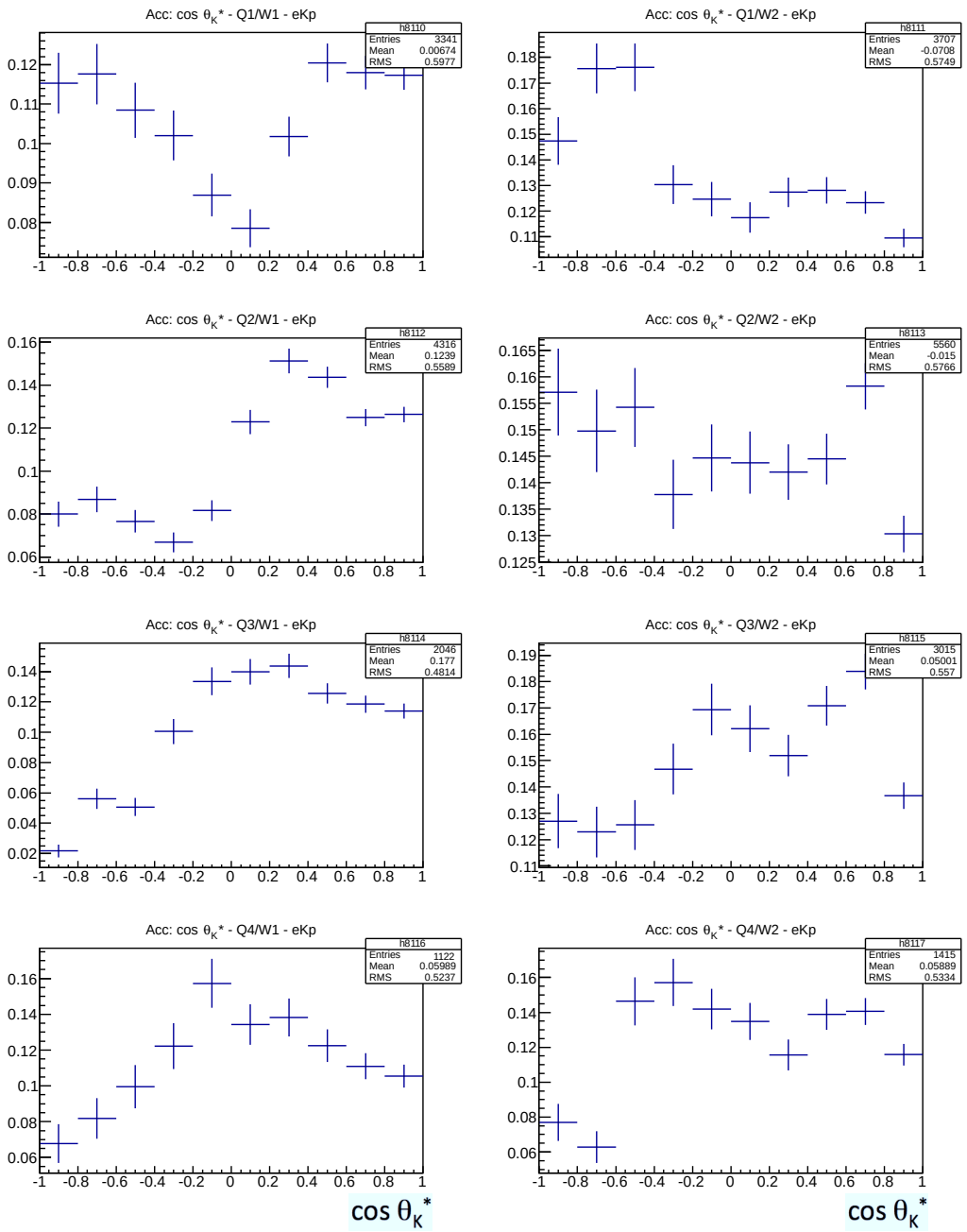

Figure 26: Acceptance functions determined from the Monte Carlo simulations for E_b=6.6 GeV with the torus set at $B = 0.9B_{max}$ for negatively charged particles outbending as a function of $\cos\theta^*_K$ averaged over Φ for the $K^+\Lambda$ final state for the $e'K^+p$ topology for W=1.725 GeV (left) and W=1.925 GeV (right) for each of the four Q^2 bins listed in Table 2, Q^2=2.0 GeV^2 (top row), 3.0 GeV^2 (second row), 4.0 GeV^2 (third row), and 5.0 GeV^2 (bottom row). These acceptances were determined with a thrown event sample of 10M events and yield statistical uncertainties on the acceptance of a few percent.

and the corresponding expected yields were reduced by a factor of two. We would also like to make clear that these count rate estimates will be repeated later this year with the full CLAS12 GEANT-4 gemc Monte Carlo [81] with the full CLAS12 event reconstruction package [82]. Preliminary comparisons of the CLAS12 response using the fastMC code suite and the CLAS12 gemc code suite have shown to yield reasonably good correspondence.

4.7 Alternative Topologies

The main emphasis of this proposal is a detailed study of the associated production of the ground state hyperons through the reactions:

$$e + p \rightarrow e' + K^+ + \Lambda \tag{15}$$
$$e + p \rightarrow e' + K^+ + \Sigma^0. \tag{16}$$

These reaction channels were chosen because they have the largest cross sections and the highest acceptances of the various strangeness channels. However, the data taken for this experiment will also nicely allow for studies of strangeness channels with smaller cross sections and detector acceptances. Among the considered reactions include:

$$e + p \rightarrow e' + K^{*+} + \Lambda \tag{17}$$
$$e + p \rightarrow e' + K^{*+} + \Sigma^0 \tag{18}$$
$$e + p \rightarrow e' + K^+ + \Lambda(1405) \tag{19}$$
$$e + p \rightarrow e' + K^+ + \Lambda(1520) \tag{20}$$
$$e + p \rightarrow e' + K^+ + \Sigma^0(1385) \tag{21}$$
$$e + p \rightarrow e' + K^0_s + \Sigma^+ \tag{22}$$
$$e + p \rightarrow e' + K^{*0} + \Sigma^+. \tag{23}$$

The yield estimates for each of these reactions were made relative to the yield for the $K^+\Lambda$ reaction. As no electroproduction cross sections are yet available, the photoproduction cross sections were extrapolated using the form of Eq.(13). The acceptance function of CLAS12 for the different final states used the same fastMC code suite discussed in Section 4.4 with a phase space model governing the energy and angular distribution of the final state particles.

Given the lower yields for analysis, it will certainly be the case that larger bin sizes in Q^2, W, and $\cos\theta^*_K$ will be required relative to those selected for the K^+Y channels. Unless the expected cross sections are substantially larger from the estimates considered here, the measurements will in all likelihood be limited to differential cross sections only. However, attempts to perform Φ fits to extract the structure functions can possibly be made in some cases, such as bins at low Q^2 and forward kaon CM angles.

4.7.1 Group A - $ep \rightarrow e'K^{*+}Y$

Present coupled channel analyses have been focused mainly on fits to data of πN, ηN, and KY production. However, studies of the K^*Y channels (see Eq.(17) and Eq.(18)) are also

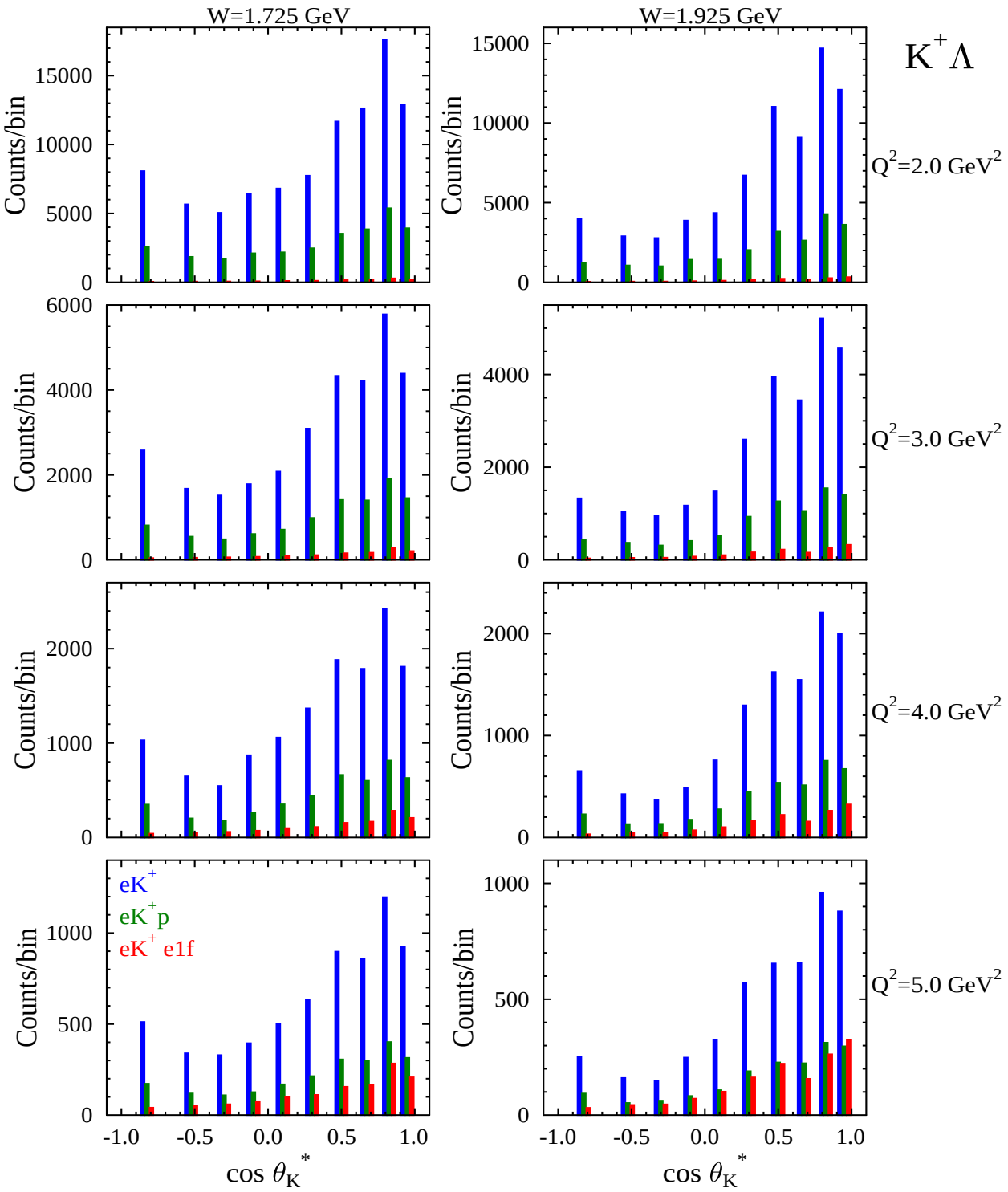

Figure 27: Expected counts in the eight bins of Table 2 at Q^2=2.0 GeV^2, 3.0 GeV^2, 4.0 GeV^2, and 5.0 GeV^2 for the $K^+\Lambda$ final state for E_b=6.6 GeV with the torus set at $B = 0.9B_{max}$ for negatively charged particles outbending at two representative values of W=1.725 GeV (left) and 1.925 GeV (right) averaged over Φ for a 50 day run at a luminosity of 1×10^{35} cm^{-2}s^{-1} for the $e'K^+$ topology (blue bars) and $e'K^+p$ topology (green bars) compared to the $e'K^+$ yields from the e1f experiment at Q^2=1.8 GeV^2 (red bars) of Ref. [44].

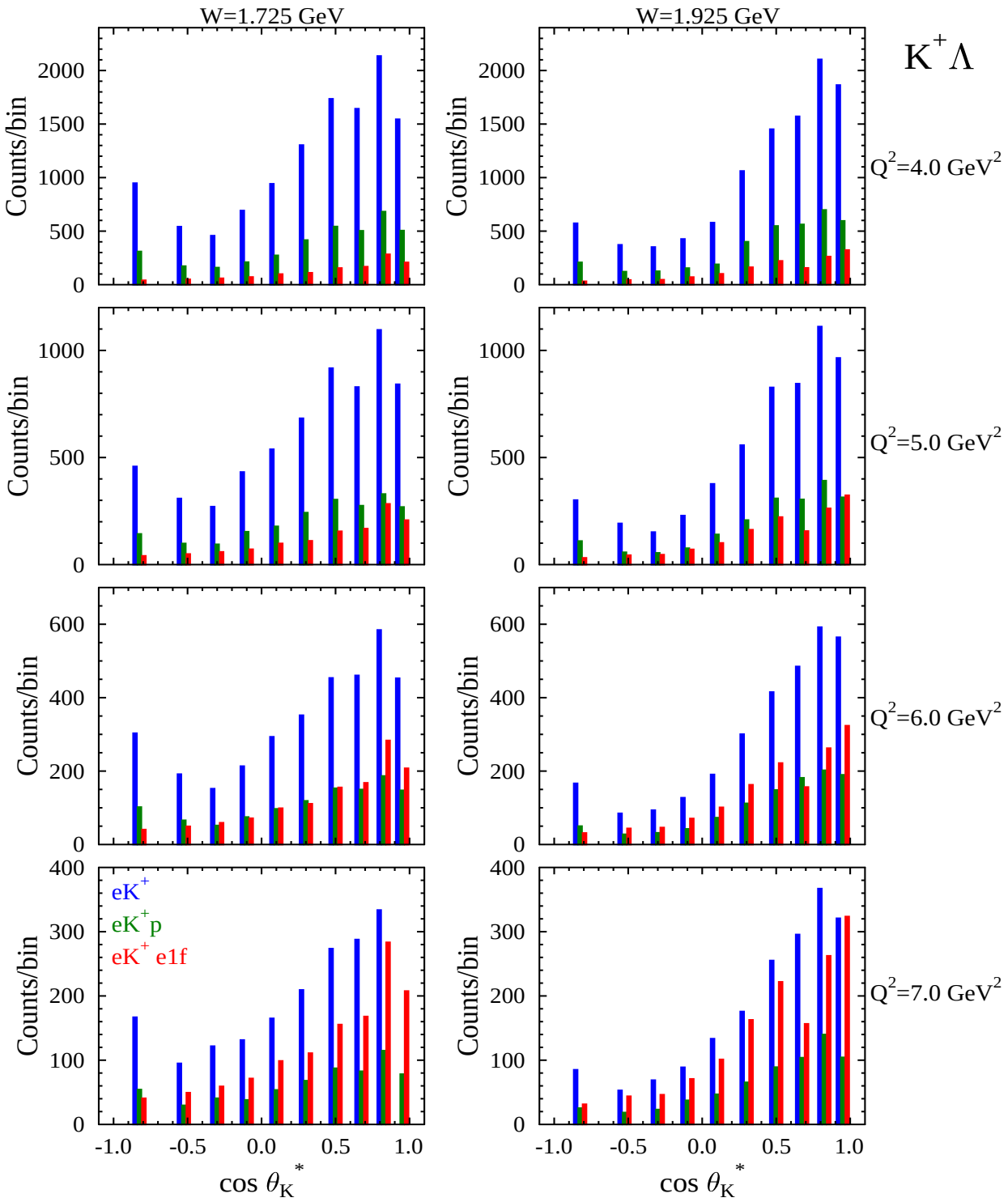

Figure 28: Expected counts in the eight bins of Table 2 at Q^2=4.0 GeV^2, 5.0 GeV^2, 6.0 GeV^2, and 7.0 GeV^2 for the $K^+\Lambda$ final state for E_b=8.8 GeV with the torus set at $B = 0.9B_{max}$ for negatively charged particles outbending at two representative values of W=1.725 GeV (left) and 1.925 GeV (right) averaged over Φ for a 50 day run at a luminosity of 1×10^{35} cm^{-2}s^{-1} for the $e'K^+$ topology (blue bars) and $e'K^+p$ topology (green bars) compared to the $e'K^+$ yields from the e1f experiment at Q^2=1.8 GeV^2 (red bars) of Ref. [44].

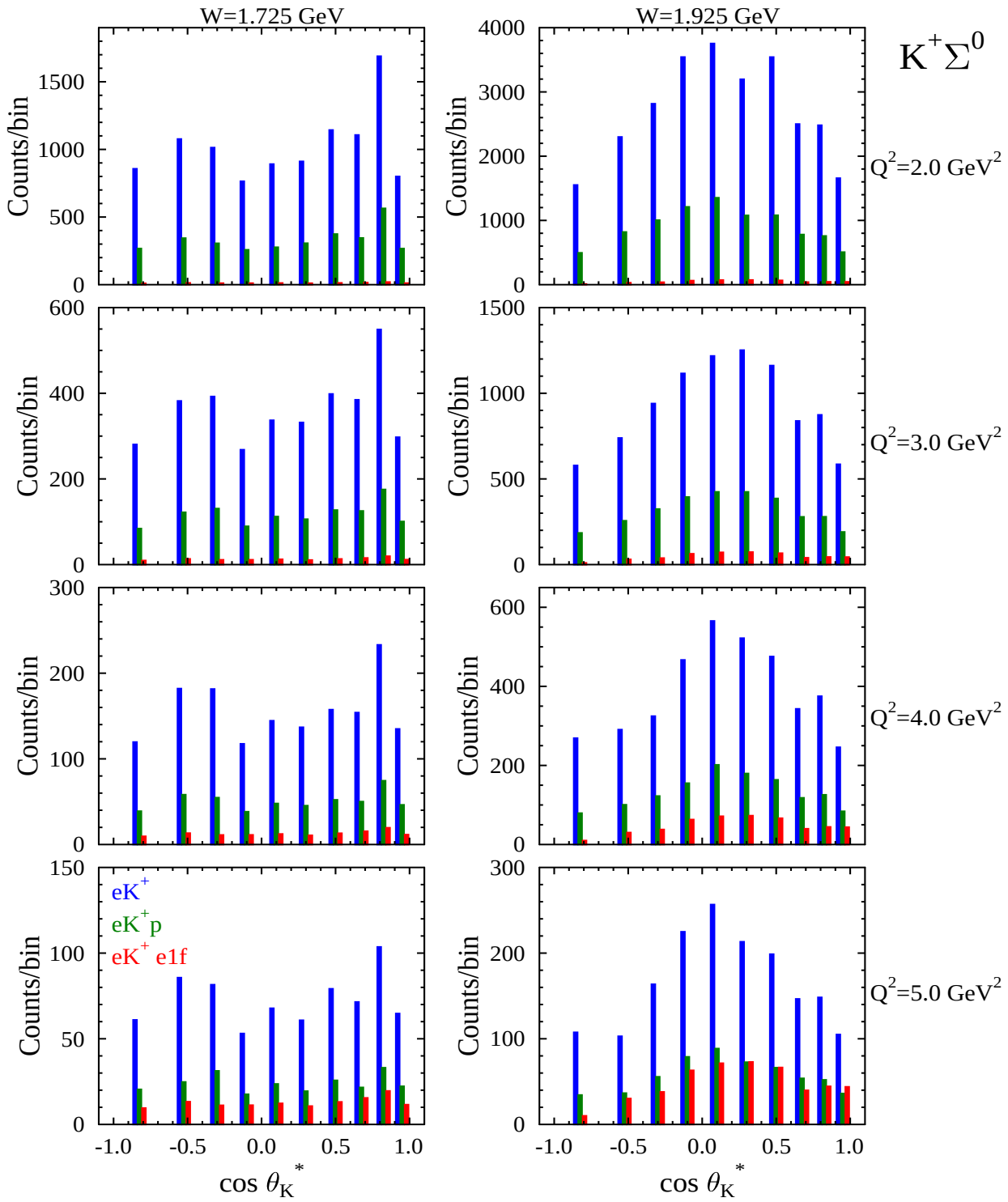

Figure 29: Expected counts in the eight bins of Table 2 at Q^2=2.0 GeV^2, 3.0 GeV^2, 4.0 GeV^2, and 5.0 GeV^2 for the $K^+\Sigma^0$ final state for E_b=6.6 GeV with the torus set at $B = 0.9B_{max}$ for negatively charged particles outbending at two representative values of W=1.725 GeV (left) and 1.925 GeV (right) averaged over Φ for a 50 day run at a luminosity of 1×10^{35} cm^{-2}s^{-1} for the $e'K^+$ topology (blue bars) and $e'K^+p$ topology (green bars) compared to the $e'K^+$ yields from the e1f experiment at Q^2=1.8 GeV^2 (red bars) of Ref. [44].

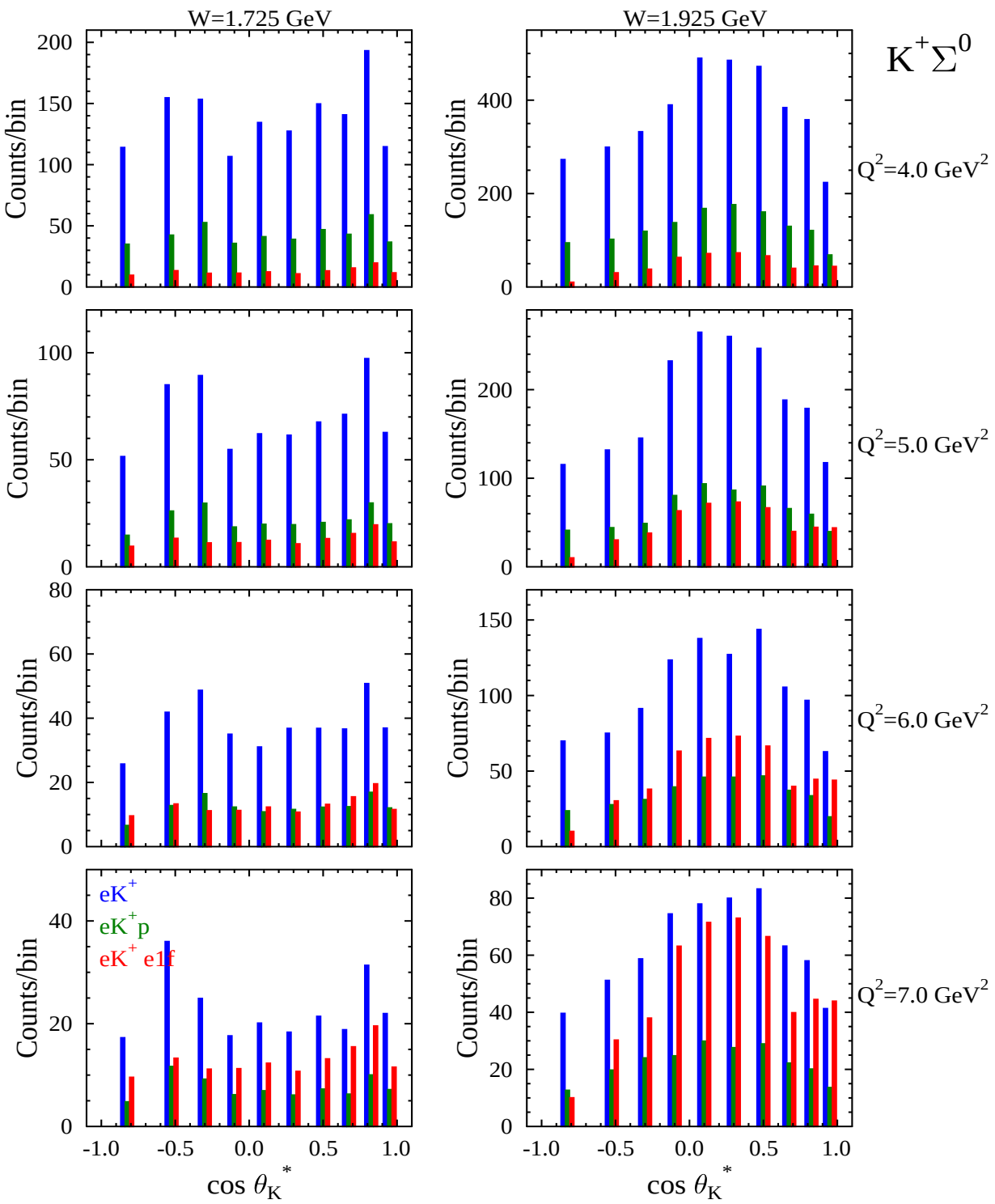

Figure 30: Expected counts in the eight bins of Table 2 at Q^2=4.0 GeV^2, 5.0 GeV^2, 6.0 GeV^2, and 7.0 GeV^2 for the $K^+\Sigma^0$ final state for E_b=8.8 GeV with the torus set at $B = 0.9B_{max}$ for negatively charged particles outbending at two representative values of W=1.725 GeV (left) and 1.925 GeV (right) averaged over Φ for a 50 day run at a luminosity of 1×10^{35} cm^{-2}s^{-1} for the $e'K^+$ topology (blue bars) and $e'K^+p$ topology (green bars) compared to the $e'K^+$ yields from the e1f experiment at Q^2=1.8 GeV^2 (red bars) of Ref. [44].

Group	Reaction	$\langle d\sigma/d\Omega\rangle$ (nb/sr)	$\langle ACC\rangle$	Yield Ratio
	$e+p \to e' + K^+ + \Lambda$	200	55%	1.000
	$e+p \to e' + K^+ + \Sigma^0$	50	55%	0.250
A	$e+p \to e' + K^{*+} + \Lambda$	10	6%	0.005
	$e+p \to e' + K^{*+} + \Sigma^0$	10	6%	0.005
	$e+p \to e' + K^+ + \Lambda(1405)$	10	11%	0.010
B	$e+p \to e' + K^+ + \Lambda(1520)$	20	10%	0.019
	$e+p \to e' + K^+ + \Sigma^0(1385)$	40	5%	0.017
C	$e+p \to e' + K^0_s + \Sigma^+$	10	6%	0.006
	$e+p \to e' + K^{*0} + \Sigma^+$	10	6%	0.006

Table 3: Yield ratio estimates for various strangeness channels considered in this proposal relative to the $K^+\Lambda$ final state in the $e'K^+$ topology. The cross section column is the expected cross section for the different channels at Q^2=1.8 GeV^2. The average acceptance column takes into account the branching ratios for the reconstructed final state(s) considered.

expected to provide unique and relevant information regarding production of high-lying N^* states. The quark model calculations of Ref. [83] showed that several N^* states are predicted to couple to the KY and K^*Y channels with similar strength. These include the $N(2080)\frac{3}{2}^-$, $N(2090)\frac{1}{2}^-$, and $N(2190)\frac{7}{2}^-$. Comparisons of the K^+Y and $K^{*+}Y$ cross sections for these states will be relevant to study the different production mechanisms involved.

The reconstruction of the $K^{*+}\Lambda$ and $K^{*+}\Sigma^0$ final states will proceed through identification of the final state K^{*+} with the hyperon identified using the missing-mass technique. The K^{*+} will be identified from the decay:

$$\begin{aligned} K^{*+} \to \quad & K^0_s\ \pi^+ \qquad (B.R. = 50\%) \\ & \hookrightarrow K^0_s \to \pi^+\pi^- \quad (B.R. = 69.2\%). \end{aligned} \tag{24}$$

The reconstructed reaction is: $ep \to e'\pi^+\pi^-\pi^+(\Lambda)$ or $ep \to e'\pi^+\pi^-\pi^+(\Sigma^0)$.

The cross section estimates for these channels are based on extrapolations from the CLAS photoproduction data from Ref. [84]. The typical cross sections averaged over W and $\cos\theta^*_{K^*}$ at the photon point are 16 nb/sr. The average CLAS12 acceptance for this reaction, accounting for the relevant branching fractions, is estimated to be ∼6%.

4.7.2 Group B - $ep \to e'K^+Y^*$

The $\Lambda(1405)$ is situated just below the $N\bar{K}$ threshold and has been an enigmatic state in the spectrum of strange baryons for many years. Only recently have precision photoproduction data from CLAS become available that have started to shed some light on the production dynamics [85, 86]. The $\Lambda(1405)$ sits between the $\Sigma(1385)$ and the $\Lambda(1520)$ hyperons. Simultaneous studies of all three states should be expected to yield insight into their production dynamics, which should lead to further insight into their structures. To date the available theoretical models that have studied $N^* \to KY^*$ decays have produced mixed results on whether s-channel resonance contributions play any significant role [87, 88, 89, 90].

The reconstruction of the three K^+Y^* channels (see Eq.(19), Eq.(20), and Eq.(21)) was considered as follows:

$$ep \rightarrow e'K^+\,\Lambda(1405) \tag{25}$$
$$\hookrightarrow\ \Lambda(1405) \rightarrow \pi^-\Sigma^+ \qquad (B.R. = 18\%) \tag{26}$$
$$\hookrightarrow\ \Lambda(1405) \rightarrow \pi^+\Sigma^- \qquad (B.R. = 18\%) \tag{27}$$

The reconstructed reactions are: $ep \rightarrow e'K^+\pi^-(\Sigma^+)$ and $ep \rightarrow e'K^+\pi^+(\Sigma^-)$.

$$ep \rightarrow e'K^+\,\Lambda(1520) \tag{28}$$
$$\hookrightarrow\ \Lambda(1520) \rightarrow K^-p \qquad (B.R. = 50\%) \tag{29}$$

The reconstructed reactions are: $ep \rightarrow e'K^+K^-(p)$ and $ep \rightarrow e'K^+p(K^-)$.

$$ep \rightarrow e'K^+\,\Sigma^0(1385) \tag{30}$$
$$\hookrightarrow\ \Sigma^0(1385) \rightarrow \Lambda\pi^0 \qquad (B.R. = 87\%) \tag{31}$$
$$\hookrightarrow \Lambda \rightarrow p\pi^- \qquad (B.R. = 64\%) \tag{32}$$

The reconstructed reaction is: $ep \rightarrow e'K^+p\pi^-(\pi^0)$.

As no electroproduction cross sections are yet available for these final states, extrapolations of the available CLAS photoproduction cross sections of Ref. [86] were employed. The typical cross sections averaged over W and $\cos\theta^*_K$ at the photon point are 16 nb/sr for $K^+\Lambda(1405)$, 32 nb/sr for $K^+\Lambda(1520)$, and 65 nb/sr for $K^+\Sigma^0(1385)$. The average CLAS12 acceptances for these reactions, accounting for the relevant branching fractions are estimated to be 11% for $K^+\Lambda(1405)$, 10% for $K^+\Lambda(1520)$, and 5% for $K^+\Sigma^0(1385)$.

4.7.3 Group C - $ep \rightarrow e'K^{(*)0}\Sigma^+$

Study of the strangeness production of different isospin partners in the final state, namely Σ^+ production vs. Σ^0 production (see Eq.(23)), is also a necessary part of developing complete reaction models. For example, the dynamics of K^{*0} production are simplified relative to K^{*+} production as K^{*0} exchange in the t-channel is strongly suppressed [91]. Thus studies of both the charged and neutral mesons in the final state may allow for scrutiny of the developed reaction models that can give additional insight into the different isospin channels and their coupling to the final state N^*s.

The reconstruction of these $K^{(*)0}\Sigma^+$ channels was considered as follows:

$$ep \rightarrow e'\,K^0_s\,\Sigma^+ \tag{33}$$
$$\hookrightarrow K^0_s \rightarrow \pi^+\pi^- \qquad (B.R. = 69\%) \tag{34}$$

The reconstructed reaction is: $ep \rightarrow e'\pi^+\pi^-(\Sigma^+)$.

$$ep \rightarrow e'\, K^{*0}\, \Sigma^+ \tag{35}$$

$$\hookrightarrow\ K^{*0} \rightarrow K^+\pi^- \qquad (B.R. = 67\%) \tag{36}$$

The reconstructed reaction is: $ep \rightarrow e'K^+\pi^-(\Sigma^+)$.

The cross section for the $K^0_s\Sigma^+$ reaction was based on available CLAS photoproduction data from Ref. [84]. The typical value averaged over W and $\cos\theta^*_K$ is 16 nb/sr. For the $K^{*0}\Sigma^+$ channel, the average cross section from CLAS photoproduction data of Ref. [92] over W and $\cos\theta^*_K$ is estimated to be 16 nb/sr. The average CLAS12 acceptances for these reactions was found to be 6%.

4.8 Systematic Uncertainties

To obtain the differential cross sections, the yields for the $K^+\Lambda$ and $K^+\Sigma^0$ final states will be extracted from the missing-mass spectra in bins of Q^2, W, $\cos\theta^*_K$, and Φ. The yields will be corrected for the acceptance function of CLAS12 including the various efficiency factors, radiative effects, and bin-centering factors. Finally, the virtual photon flux factor, the bin volume corrected for kinematic limits, and the beam-target luminosity will be divided out to obtain the cross section. Each of these factors is subject to systematic uncertainty. The systematic uncertainties are typically estimated by repeating a procedure in a slightly different way, e.g. by varying a cut parameter within reasonable limits, by employing an alternative algorithm, or by using a different model to extract a correction, and noting how the results change. This similar approach is applicable for the Φ moment analysis to extract the separated structure functions from the differential cross sections and for the asymmetry fits to extract the induced and beam-transferred hyperon polarizations. The procedures to estimate the systematic uncertainties for each of these observables are discussed in detail in our CLAS publications [42, 43, 44, 45, 46, 47].

Based on our experience from analysis of CLAS data to extract cross sections and polarization observables, there are five categories of systematic uncertainty. These include yield extraction, detector acceptance and efficiencies, radiative corrections, bin centering corrections, and scale uncertainties. Table 4 lists the categories, specific sources, and the systematic uncertainties that are expected from the proposed measurements of the differential cross sections. Overall the scale of the systematic uncertainties is at the level of about 10%. A 10% systematic uncertainty is also typical for what might be expected for the hyperon polarization measurements based on experience with analysis of data from CLAS. Of course, as the CLAS12 spectrometer has not yet been made available for physics running and we have no operational experience with this system, the estimates contained in Table 4 are preliminary estimates that might be considered as reasonable given past experience.

5 Summary and Beam Time Request

The studies of the electromagnetic transition amplitudes between the nucleon ground and excited states over a wide range of Q^2 elucidate the relevant degrees of freedom in the N^* structure at different distance scales and will allow for a better understanding of the non-perturbative strong interaction that governs the formation of the N^* states. With the JLab

Category	Systematic Uncertainty
1. Yield Extraction	
Fiducial cuts	0.5-3%
Electron identification	0.5%
2. Detector Acceptance	
MC model dependence	2-5%
Tracking efficiencies	5%
Close track efficiencies	1%
CC efficiency function	0.5-2%
3. Radiative Corrections	2%
4. Bin Centering	0.5%
5. Scale Uncertainties	
Beam polarization	2%
Beam Charge Asymmetry	<0.2%
Photon flux factor	3%
Luminosity	3%
Total	10%

Table 4: Categories and expected systematic uncertainties for the differential cross sections for the proposed measurements. The total systematic uncertainty assignment is obtained by adding the different contributions in quadrature. The beam polarization systematic is only relevant for the extraction of $\sigma_{LT'}$ and the transferred hyperon polarization components.

12-GeV upgrade and the new CLAS12 detector, a unique opportunity is available to probe the structure of nucleon resonances over a broad range of Q^2.

In recent years the CLAS Collaboration has succeeded in determining the Q^2 evolution of baryon resonance electrocoupling amplitudes from unpolarized $N\pi$ and $N\pi\pi$ electroproduction data. These studies make clear that the independent analysis of multiple final states in the same kinematic domain is essential to minimize the systematics of the measurements and to have confidence in the extracted electrocoupling parameters. In terms of pionic coupling, most high-lying N^* states preferentially decay through the $N\pi\pi$ channel instead of the $N\pi$ channel. Thus data from the KY channels is critical to provide an independent extraction of the electrocoupling amplitudes for the high-lying N^* states against those determined from the analysis of the $N\pi\pi$ channel.

The CLAS12 N^* program already consists of two approved experiments. E12-09-003 [6] will focus on studies of N^* states from the single non-strange meson and $N\pi\pi$ channels. E12-06-108A [7] will focus specifically on the study of N^* states from the strangeness channels with a focus on the exclusive $K^+\Lambda$ and $K^+\Sigma^0$ reactions. Both E12-09-003 and E12-06-108A are part of the first physics running period with CLAS12 that will employ a longitudinally polarized 11 GeV electron beam. These two experiments seek to extract the electrocouplings of all prominent N^* and Δ^* excited states spanning the full nucleon resonance region up to W=3 GeV in the almost unexplored region of Q^2 from 5 GeV^2 to 12 GeV^2.

This proposal extends the physics reach of the existing CLAS12 N^* program and specifically E12-06-108A through measurements of the $K^+\Lambda$ and $K^+\Sigma^0$ final states using longitudi-

nally polarized electron beams of energies E_b=6.6 GeV and 8.8 GeV. The Q^2 coverage from 2 GeV^2 to 7 GeV^2 covered by the data from this proposal makes this extension of the N^* program the most suitable for the exploration of the emergence of the outer meson-baryon cloud in the structure of N^* states from the regime of quark-gluon confinement. These data will allow for precision measurements of cross sections and separated structure functions σ_U, σ_{LT}, σ_{TT}, and $\sigma_{LT'}$, as well as the induced and beam-recoil transferred hyperon polarizations in the Q^2 range from 2 GeV^2 to 7 GeV^2.

The count rate estimates have been carried out assuming 50 days of data taking at both 6.6 GeV and 8.8 GeV beam energies. The K^+Y yields as computed from the CLAS12 fastMC simulation reconstructing the final state by detection of the e' and K^+ are expected to be nearly two orders of magnitude higher compared to those from the measurements already carried out using CLAS for Q^2 up to 4 GeV^2. In the Q^2 range from 4 GeV^2 to 7 GeV^2, the computed yields are expected to be a factor of $\sim$3 larger than what was acquired with the CLAS dataset at Q^2=1.8 GeV^2. The request of 50 days at E_b=6.6 GeV (8.8 GeV) ensures that in the highest bin of photon virtuality Q^2=5.0 GeV^2 (7.0 GeV^2), the statistics in the $e'K^+p$ ($e'K^+$) topology are comparable with those in the $e'K^+$ topology for the Q^2=1.8 GeV^2 bin for the existing CLAS data from Ref. [44].

This proposal also provides a unique opportunity to probe the electroproduction of exclusive K^*Y and KY^* final states through measurements of their differential cross sections at levels of statistical precision that have not been possible for data from the CLAS measurement program. While this is not the main emphasis of this proposal, it is felt that the data for this experiment will provide a unique opportunity that should be overlooked or bypassed.

For the foreseeable future, CLAS12 will be the only facility in the world capable of investigating the spectrum and the structure of excited nucleon states at distance scales from low to high Q^2, encompassing the regime where low-energy meson-baryon degrees of freedom dominate to the regime where the quark degrees of freedom are expected to dominate. The extraction of the $\gamma_v NN^*$ transition amplitudes for the prominent N^* and Δ^* states from the comprehensive data based on this experiment, together with those provided by the already approved N^* experiments of the 12 GeV program, will allow for the opportunity to better understand how the strong interaction of dressed quarks gives rise to the spectrum and structure of excited nucleon states, and how these states emerge from QCD.

This proposal is designed to be fully compatible with the new CLAS12 run group featuring, in additional to this experiment, the proposals to study hybrid baryons and deeply virtual Compton scattering, running with 100 days of total beam time. These experiments will use longitudinally polarized electron beams with the highest possible polarization at electron beam energies of 6.6 GeV and 8.8 GeV with an unpolarized liquid-hydrogen target at a beam-target luminosity of $\mathcal{L} = 1 \times 10^{35}$ cm^{-2}s^{-1} with the maximum torus current operated with negatively charged particles outbending. We request that the JLab PAC approve this experiment as part of the Jefferson Laboratory physics program in Hall B and recognize its importance as an extension to the existing CLAS12 N^* program at high Q^2. This proposal has been reviewed internally within the CLAS Collaboration and has been fully endorsed by the CLAS Collaboration.

The participation of the different research groups that are a part of this proposal has

been fully detailed in the proposal for E12-06-108A [7] and is listed in Section 6. The data collected as part of this lower energy running will be considered another aspect of the existing effort.

6 Participation of Research Groups

Jefferson Laboratory

The Hall B Group will have significant responsibility for overall organization of the run, oversight of the data collection and data processing, and will lead many aspects of the Stage 1 and Stage 2 analyses described in Section 4.2 and 4.3. Daniel Carman is a lead author on nearly all of the CLAS KY electroproduction papers. Victor Mokeev has been the driving force behind the efforts to extract the electrocouplings from the CLAS $N\pi$ and $N\pi\pi$ final states. Kijun Park lead the analysis of the separated structure functions for the $N\pi$ CLAS data with the subsequent extraction of the electrocoupling parameters for resonances in the region of W=1.6 GeV. Volker Burkert has been the driving force behind the entire N^* program in Hall B from its inception. Each of these contributors will be involved in multiple aspects of the analysis of the data to extract observables and the higher-level analysis to extract the electrocoupling parameters.

University of South Carolina

Ralf Gothe from the University of South Carolina is not only a spokesperson of this proposal, but also is a spokesperson of the related CLAS12 N^* experiments as part of E12-09-003 and E12-06-108A. He will be involved in not only data analysis issues pertaining to this data set, but also on working to develop the associated reaction models and the fitting algorithms for the higher-level analysis that will ultimately be required for extraction of the electrocoupling parameters of the N^* resonance states. Ralf Gothe's group was also responsible for the assembly and calibration of the high resolution FTOF panel-1b counters that represent the main subsystem to be employed for charged particle identification in this experiment.

Center for Nuclear Studies - GW Data Analysis Center

The George Washington University Data Analysis Center is actively involved in an extensive research program on the theoretical interpretation of the results from the proposed experiment. In particular, the GW group will provide an extended analysis of the πN, NN, KY, γN, and $\gamma^* N$ processes on the time scale of the completion of this experiment.

Lattice Group at the JLab Theory Center

Members of the Lattice Group at the JLab Theory Center are actively involved in an extensive research program on the theoretical interpretation of the results from the proposed experiment. In particular, the group will provide LQCD calculations of transition helicity amplitudes and/or related form factors for several excited proton states of various quantum numbers at photon virtualities of the proposed experiment on the time scale the completion of this experiment.

JLab Physics Analysis Center

The JLab Physics Analysis Center that was formed after the culmination of the Excited Baryon Analysis Center (EBAC) is actively involved in an extensive research program on the theoretical interpretation of the results from the proposed experiment. In particular, this

group will help to develop analysis methods for interpreting the extracted N^* form factors for Q^2 up to 12 GeV^2 (which encompasses the full set of related experiments from both CLAS and CLAS12) in terms of DSE and LQCD predictions on the time scale of the completion of this experiment.

Argonne-Osaka Group

Members of the Argonne-Osaka Group are actively engaged in extending the analysis of meson production amplitudes through their dynamical coupled-channel approach that was started under the aegis of the JLab Excited Baryon Analysis Center (EBAC). This group is working to extract the mass, coupling constants, and electromagnetic transition form factors of the N^* states across the full resonance region at photon virtualities relevant for this experiment on a time scale compatible with the completion of this experiment.

Argonne National Lab

The Argonne National Lab (ANL) contributors to this proposal are actively involved in an extensive research program on the theoretical interpretation of the results from the proposed experiment. In particular, ANL group will provide calculations of transition helicity amplitudes and/or related form factors for several excited proton states of various quantum numbers within the framework Dyson-Schwinger on the time scale of the completion of this experiment.

Ghent University

Members of the Ghent group are actively involved in the development of reaction models for KY electroproduction that are being employed as the basis for the development of a complete model that will be used to describe the KY energy and angular of distributions this experiment and of the existing KY electroproduction data from CLAS at lower Q^2. This model will be employed to extract the electrocoupling parameters for the dominant N^* and Δ^* states coupling to the strangeness channels.

Florida International University

Brian Raue from Florida International University is a lead author on the majority of the CLAS KY electroproduction papers from the analysis of the separated structure functions, to the extraction of the single and double polarization observables. He will be involved in multiple aspects of the data analysis for this experiment.

Moscow State University

The Moscow State University group will participate in the development of the simulation (GEANT-4) and reconstruction software, trigger, and data acquisition. MSU will develop and support the special database needed for N^* studies in the coupled-channel analysis.

University of Iowa

Haiyun Lu from the University of Iowa has been involved as a lead author on analysis of CLAS KY^* photoproduction data. He will be involved in multiple aspects of the data

analysis for this experiment.

Ohio University

Ken Hicks from Ohio University has been involved in the CLAS strangeness physics program as a lead author on the analysis of data for the $K^{*+}Y$ and $K^{*0}Y$ channels in photoproduction. He has also played an important role in related analysis and publications as a collaborator at LEPS and is a spokesperson on JPARC experiment P45. He will be involved in multiple aspects of the data analysis for this experiment.

University of Glasgow

Dave Ireland from the University of Glasgow has been heavily involved in leading the analysis on the extraction of observables from the CLAS g7/FROST dataset and has also worked on the development of the RPR model with the University of Ghent group. He will be involved in multiple aspects of the data analysis and model development for this experiment.

Universitá di Roma

Annalisa D'Angelo and her group have been involved in the CLAS N^* program studying the data from the g14/HD-Ice run period. The Rome group will be involved in the organization and oversight of the run period and with multiple aspects related to data analysis and fitting.

INFN Sezione di Genova

Elena Santopinto will provide theoretical support to the Stage 2 portion of the analysis including the development of quark models with consideration of the N^* states and electrocouplings derived from these data.

References

[1] N. Isgur and G. Karl, Phys. Rev. D **19**, 2653 (1979).

[2] S. Capstick and N. Isgur, Phys. Rev. D **34**, 2809 (1986).

[3] I.G. Aznauryan and V.D. Burkert, Prog. Part. Nucl. Phys. **67**, 1 (2012).

[4] H. Kamano, S.X. Nakamura, T.-S.H. Lee, and T. Sato, Phys. Rev. C **88**, 035201 (2013).

[5] I.G. Aznauryan *et al.*, Int. J. Mod. Phys. **E22**, 1330015 (2013).

[6] JLab Experiment E12-09-003, spokespersons: V.D. Burkert, P. Cole, R. Gothe, K. Joo, V. Mokeev, P. Stoler

[7] JLab Experiment E12-06-108A, spokespersons: D.S. Carman, R. Gothe, V. Mokeev

[8] C.D. Roberts, arXiv:1509.02925, (2015).

[9] C.D. Roberts, J. Phys. Conf. Ser.**630**, 012051 (2015).

[10] V. Pascalutsa, M. Vanderhaeghen, and S.N. Yang, Phys. Rept. **437**, 125 (2007).

[11] M.V. Polyakov and K.M. Semenov-Tian-Shansky, Eur. Phys. J. A **40**, 181 (2009).

[12] J. Segovia *et al.*, Phys. Rev. Lett. **115**, 171801 (2015).

[13] I.C. Cloët and C.D. Roberts, Prog. Part. Nucl. Phys. **77**, 1 (2014).

[14] I.V. Anikin *et al.*, Phys. Rev. D **92**, 014018 (2015).

[15] White Paper of the JLab Workshop, *"Electromagnetic N-N* Transition Form Factors"*, Newport News, VA, USA, October 13-15, 2008.

[16] U. Löhring, B.C. Metsch, and H.R. Petry, Eur. Phys. J. A **10**, 395 (2001).

[17] J.J. Dudek and R.G. Edwards, Phys. Rev. D **85**, 054016 (2012); J.J. Dudek, EPJ Web Conf. **73**, 01004 (2014).

[18] J. Beringer *et al.* (PDG), Phys. Rev. D **86**, 010001 (2012).

[19] B. Julia-Diaz, D.O. Riska, and F. Coester, Phys. Rev. C **79**, 035212 (2004).

[20] I.G. Aznauryan, Phys. Rev. C **76**, 025212 (2007).

[21] I.G. Aznauryan and V.D. Burkert, Phys. Rev. C **85**, 055202 (2012).

[22] I.G. Aznauryan and V.D. Burkert, arXiv:1603.06692, (2016).

[23] C.S. An *et al.*, Phys. Rev. C **74** 055205 (2006).

[24] M. Aiello, M.M. Giannini, and E. Santopinto, J. Phys. G **24**, 753 (1998)

[25] M. De Sanctis *et al.*, Phys. Rev. C **76**, 062202 (2007).

[26] M. Bhagwat and P. Tandy, AIP Conf. Proc. **842**, 225 (2006).

[27] C.D. Roberts, Prog. Part. Nucl. Phys. **61**, 55 (2008).

[28] C. Chen *et al.*, Few Body Syst. **53**, 293 (2012).

[29] I.C. Cloët and C.D. Roberts, Prog. Part. Nucl. Phys. **77**, 1 (2014).

[30] C.D. Roberts, arXiv:1509.08952 (nucl-th), (2015).

[31] J. Segovia *et al.*, Few Body Syst. **55**, 1185 (2014).

[32] USQCD Collaboration, http://www.usqcd.org/collaboration.html.

[33] Jefferson Laboratory Joint Physics Analysis Center, https://jpac.jlab.org/.

[34] B.A. Mecking *et al.*, Nucl. Inst. and Meth. A **503**, 513 (2003).

[35] V.I. Mokeev and I.G. Aznauryan, Int. J. Mod. Phys. Conf. Ser. **26**, 1460080 (2014).

[36] V.I. Mokeev. Presentation at the ECT* Workshop, *Nucleon Resonances: From Photoproduction to High Photon Virtualities*, (2015).

[37] V.I. Mokeev *et al.*, Phys. Rev. C **93**, 025206 (2016).

[38] I.G. Aznauryan *et al. (CLAS Collaboration)*, Phys. Rev. C **80**, 055203 (2009).

[39] K. Park *et al. (CLAS Collaboration)*, Phys. Rev. C **91**, 045203 (2015).

[40] I.G. Aznauryan and V.D. Burkert, Phys. Rev. C **92**, 015203 (2015).

[41] B.A. Raue and D.S. Carman, Phys. Rev. C **71**, 065209 (2005).

[42] P. Ambrozewicz *et al. (CLAS Collaboration)*, Phys. Rev. C **75**, 045203 (2007).

[43] R. Nasseripour *et al. (CLAS Collaboration)*, Phys. Rev. C **77**, 065208 (2008).

[44] D.S. Carman *et al. (CLAS Collaboration)*, Phys. Rev. C **87**, 025204 (2013).

[45] M. Gabrielyan *et al. (CLAS Collaboration)*, Phys. Rev. C **90**, 035202 (2014).

[46] D.S. Carman *et al. (CLAS Collaboration)*, Phys. Rev. Lett. **90**, 131804 (2003).

[47] D.S. Carman *et al. (CLAS Collaboration)*, Phys. Rev. C **79**, 065205 (2009).

[48] CLAS physics database, http://clasweb.jlab.org/physicsdb.

[49] O. Maxwell, Phys. Rev. C **85**, 034611 (2012).

[50] T. Corthals *et al.*, Phys. Lett. B **656**, 186 (2007).

[51] L. De Cruz *et al.*, Phys. Rev. C **86**, 015212 (2012).

[52] A.V. Anisovich *et al.*, Eur. Phys. J A **48**, 15 (2012).

[53] E. Klempt and R. Workman, https://pdg.web.cern.ch/pdg/2012/reviews/rpp2012-rev-n-delta-resonances.pdf.

[54] V.A. Nikonov *et al.*, Phys. Lett. B **662**, 245 (2008).

[55] B. Julia-Diaz *et al.*, Nucl. Phys. A **755**, 463 (2005); B. Julia-Diaz *et al.*, Phys. Rev. C **73**, 055204 (2006).

[56] T. Mart and A. Sulaksono, Phys.Rev. C **74**, 055203 (2006).

[57] A.V. Anisovich *et al.*, Eur. Phys. J. A **48**, 88 (2012).

[58] P.O. Bowman *et al.*, Phys. Rev. D **71**, 054507 (2005).

[59] I.C. Cloët, C.D. Roberts, and A.W. Thomas, Phys. Rev. Lett **111**, 101803 (2013).

[60] L.L. Frankfurt *et al.*, Phys. Rev. Lett. **84**, 2589 (2000).

[61] K. Goeke, M.V. Polyakov, and M. Vanderhaeghen, Prog. Part. Nucl. Phys. **47**, 401 (2001).

[62] I.V. Anikin, V.M. Braun, N. Offen, Phys. Rev. D **92**, 014018 (2015).

[63] CLAS12 web page, see http://www.jlab.org/Hall-B/clas12-web.

[64] G. Knöchlein, D. Drechsel, L. Tiator, Z. Phys. **A 352**, 327 (1995).

[65] S. Boffi, C. Giusti, and F.D. Pacati, Phys. Rep. **226**, 1 (1993); S. Boffi, C. Giusti, and F.D. Pacati, Nucl. Phys. A **435**, 697 (1985).

[66] C.W. Akerlof *et al.*, Phys. Rev. **163**, 1482 (1967).

[67] A. Afanasev, I. Akushevich, V. Burkert, and K. Joo, Phys. Rev. D **66**, 074004 (2002).

[68] JLab Workshop on *Precision Radiative Corrections for Next Generation Experiments*, May 16-19, 2016, https://www.jlab.org/conferences/radiatve2016/

[69] B.E. Bonner *et al.*, Phys. Rev. D **38**, 729 (1988).

[70] L. Tiator *et al.*, Eur. Phys. J. ST **198**, 141 (2011).

[71] I. Aznauryan, Phys. Rev. C **67**, 015209 (2003).

[72] V. Mokeev *et al. (CLAS Collaboration)*, Phys. Rev. C **86**, 035203 (2012).

[73] V.I. Mokeev *et al.*, Phys. Rev. C **80**, 045212 (2009).

[74] T. Vrancx, J. Ryckebusch, and J. Nys, arXiv:1404.4156, (2014).

[75] J. Nys, Presentation at the ECT* Workshop, *Nucleon Resonances: From Photoproduction to High Photon Virtualities*, (2015),
http:/boson.physics.sc.edu gothe/ect*-15program.html

[76] M. Döring, Int. J. Mod. Phys. Conf. Ser. **26**, 1460054 (2014).

[77] JPARC Experiment P45, *3-Body Hadronic Reactions for New Aspects of Baryon Spectroscopy*, K.H. Hicks and H. Sako spokesperson.

[78] R.A. Schumacher and M.M. Sargsian, Phys. Rev. C **83**, 025207 (2011).

[79] T. Sjöstrand, S. Mrenna, and P. Skands, Jour. of High Energy Phys., JHEP05, (2006).

[80] D.S. Carman, FTOF Project Close-out Slides, https://www.jlab.org/Hall-B/ftof/ftof-closeout.pdf

[81] GEMC Documentation,
see https://gemc.jlab.org/gemc/Documentation/Documentation.html

[82] CLAS12 Software Development,
see http://clasweb.jlab.org/clas12offline/docs/software/html/

[83] S. Capstick and W. Roberts, Phys. Rev. D **58**, 074011 (1998).

[84] W. Tang *et al. (CLAS Collaboration)*, Phys. Rev. C **87**, 065204 (2013).

[85] K. Moriya *et al. (CLAS Collaboration)*, Phys. Rev. C **87**, 035206 (2013).

[86] K. Moriya *et al. (CLAS Collaboration)*, Phys. Rev. C **88**, 045201 (2013).

[87] Y.Oh, C.M. Ko, and K. Nakayama, Phys. Rev. C **77**, 045204 (2008).

[88] S.-I. Nam, A. Hosaka, and H.-C. Kim, Phys. Rev. D **71**, 114012 (2005).

[89] J. He and X.-R. Chen, Phys. Rev. C **86**, 035204 (2012).

[90] S.-I. Nam, J.-H. Park, A. Hosaka, and H.-C. Kim, J. Korean Phys. Soc. **59**, 2676 (2011).

[91] Q. Zhao, J.S. Al Khalili, and C. Bennhold, Phys. Rev. C **64**, 052201 (R) (2001).

[92] I. Hleiqawi *et al. (CLAS Collaboration)*, Phys. Rev. C **75**, 042201 (R) (2007).